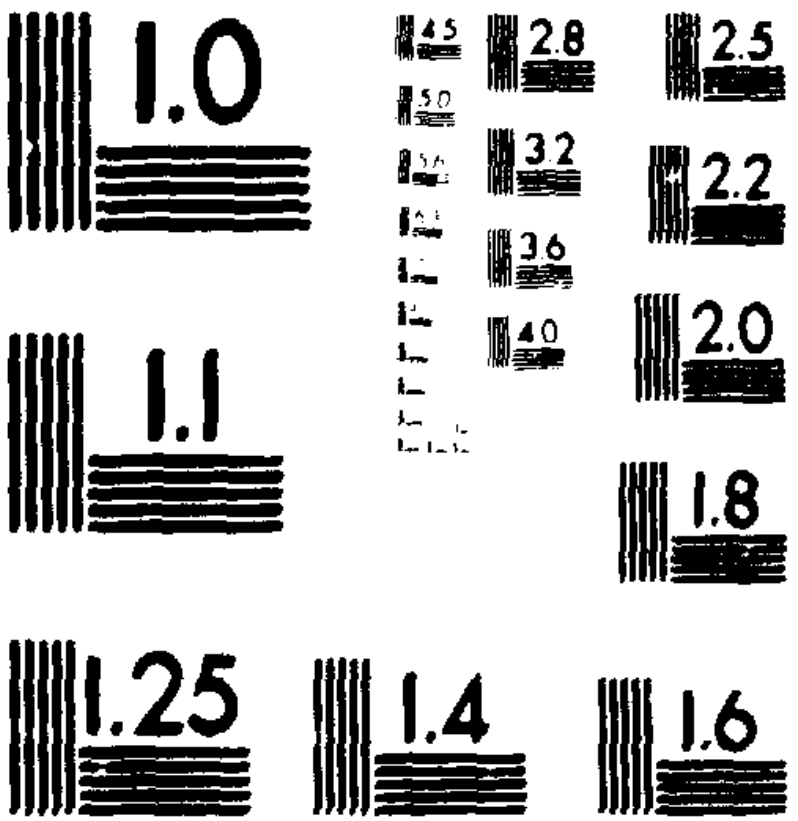

ENEA. RT/FUS/85/13

# CONTRIBUTIONS TO THE 3rd INTERNATIONAL SYMPOSIUM ON RADIATION PHYSICS

**Ferrara, September 30, 1985**



COMITATO NAZIONALE PER LA RICERCA E PER LO SVILUPPO DELL'ENERGIA NUCLEARE E DELLE ENERGIE ALTERNATIVE

COMITATO NAZIONALE PER LA RICERCA E PER LO SVILUPPO
DELL'ENERGIA NUCLEARE E DELLE ENERGIE ALTERNATIVE
ASSOCIAZIONE EURATOM-ENEA SULLA FUSIONE

# CONTRIBUTIONS TO THE 3rd INTERNATIONAL SYMPOSIUM ON RADIATION PHYSICS

**Ferrara, September 30, 1985**

R. BARTIROMO ed altri
ENEA - Dipartimento Fusione, Centro ricerche energia Frascati

RT/FUS/85/13

This report has been prepared by: Servizio Studi e Documentazione - ENEA, Centro Ricerche Energia Frascati, C.P. 65 - 00044 Frascati, Rome, Italy.

This Office will be glad to send further copies of this report on request.

CONTENTS

# X-RAY DIAGNOSTIC OF TOKAMAK PLASMA

Rosario Bartiromo

Associazione EURATOM-ENEA sulla Fusione, Centro Ricerche Energia Frascati,
C.P. 65 - 00044 Frascati, Rome, Italy.

**SUMMARY**

The basic processes responsible for the X-ray emission in tokamak plasmas are described and their diagnostic application discussed.

# 1. INTRODUCTION

The last decade has witnessed the enormous progresses obtained by tokamak machines towards the achievement of controlled thermonuclear fusion. Reactor relevant confinement time and plasma temperature have been obtained, although in different devices and under different plasma conditions, and the large tokamaks of the present generation, like JET and TFTR, are engaged in combining these conditions to obtain the first insight into the behaviour of a reacting plasma.

However many aspects of the physics of a tokamak plasma are far from being completely understood making it difficult to predict the performances of future devices on such fundamental issues like plasma confinement and heating. In this respect an important role is played by the discipline of plasma diagnostic which is called to evolve more and more sophisticately to document, besides the basic plasma parameters like for example density and temperature, more intrinsic properties like the thermal conductivity and magnetohydrodynamic stability [1].

Among the different techniques presently applied to characterize the plasma, X-ray diagnostic has proven to be one of the most versatile and fruitful. It has taken advantage from the steady increase in electron temperature obtained both in ohmically and additionally heated plasmas.

It will grow even more important in future years up to the point that, for plasma close to thermonuclear conditions, all the information usually derived from spectroscopic diagnostics will be obtained only by means of

high resolution X-ray spectroscopy. In fact, in these conditions light impurities are completely stripped and only contribute to plasma radiation through electron bremsstrahlung and recombination processes, whereas metallic impurities are highly ionized and present in the plasma core only in the hydrogen-like and helium-like ionization stages which emit line radiation only in the soft X-ray spectral region.

High resolution X-ray spectroscopy of plasmas has progressed enormously in recent years and can now be routinely applied to determine ion temperature from the Doppler width of impurity line radiation. Moreover it takes advantage from spectral features due to dielectronic recombinaiton and inner shell excitation processes to measure the electron temperature, to determine the ionization equilibrium of impurities and to study the deviation of the electron population from thermal equilibrium.

Besides the purely spectroscopic techniques, intensity measurements of plasma soft X-ray radiation in a broad energy band offer the possibility of studying fast relaxation phenomena in the plasma core, like internal disruptions, and to obtain the spatial structure of the internal magnetohydrodynamical oscillation modes. This possibility of performing very fast time resolved measurements is presently used to determine important parameters like the power deposition profile and the heat conductivity.

At the far end of the spectrum, owing to the process of relativistic bremsstrahlung, it is possible in principle, from the hard X-ray emission, to characterize completely the electron distribution function in plasmas far from the thermal equilibrium, like those produced under the condition of radiofrequency current drive.

In this paper the fundamental processes responsible for the X-ray emission of a plasma are briefly reviewed and their exploitation for diagnostic purposes is discussed. In Sec. 2 the continuous spectrum is discussed and the application of low resolution spectroscopy. Fast intensity measurements are considered in Sec. 3 and and in Sec. 4 the line emission is analyzed and the results of high resolution spectroscopy presented.

## 2. BASIC PRINCIPLES

Good surveys of X-ray plasma emission have been obtained since the beginning of tokamak research by means of proportional counters and semiconductor diode detectors [2,3]. In Fig. 1 a spectrum measured on the Frascati Tokamak FT is represented: it shows the presence of a continuous emission characterized by an exponential decay on which discrete $K_\alpha$ lines radiation from metallic impurities are superimposed. The presence of impurities in the plasma complicates the analysis of the experimental data, but on the other hand offers new opportunities to determine basic plasma parameters, as will be shown later.

Two fundamental processes are responsible for the emission of the continuous spectrum [4], namely electron ion bremsstrahlung and electron recombination on a bound level of hydrogen or impurity ion. In the following we will discuss the basic approximation usually made in plasma diagnostic to describe the X-ray continuous emission and the information that can be obtained from the experimental data.

Electron-ion bremsstrahlung in a plasma is usually computed for isotropic electron distribution function

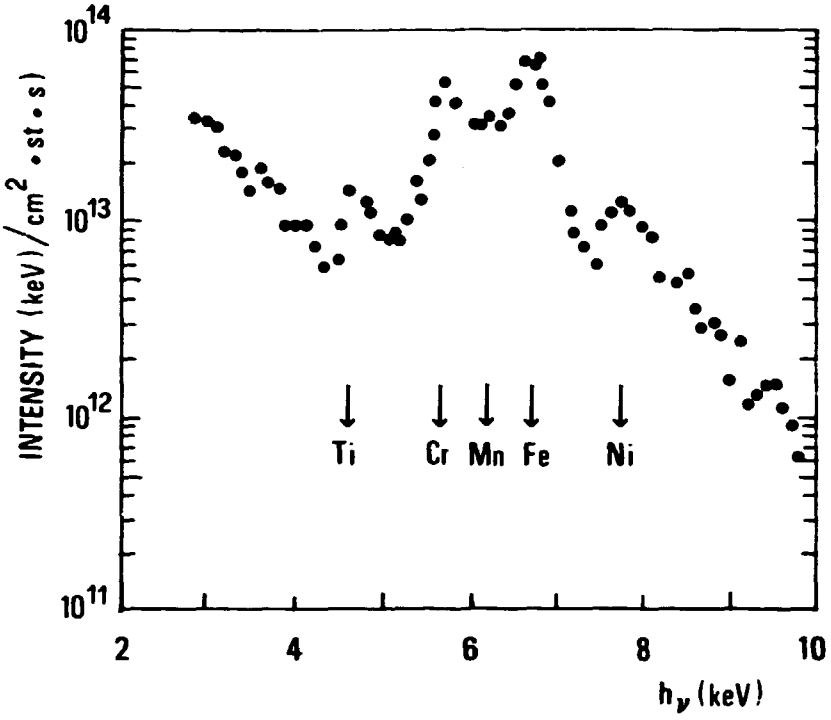


Fig.1 Soft X-ray emission spectrum from a discharge in the Frascati Tokamak FT.

(for a discussion of non-isotropic distribution see Ref.[5]). For plasma temperature lower than 10 keV, the non-relativistic Sommerfeld expression for the angle integrated cross section can be used [6].

$$\sigma(h\nu) = \frac{16}{3}\frac{\pi}{\sqrt{3}}\left(\frac{e^2}{\hbar c}\right)^3 Z^2 \frac{\hbar^2}{2m\varepsilon}\frac{g_{ff}(\varepsilon,h\nu)}{h\nu}$$

where $\varepsilon$ is the incident electron energy, $h\nu$ the emitted photon energy. The Gaunt factor $g_{ff}(\varepsilon,h\nu)$ has been derived by Sommerfeld in terms of the hypergeometric function and calculated numerically by Karzas and Latter [7] in a wide range of $\varepsilon$ and $h\nu$. Z is equal to the nuclear charge $Z_N$ when bare nuclei are considered, but for partially ionized impurity the screening of the Coulomb nuclear potential by the bound electrons has to be considered. This screening effect depends on the impact parameter: for distant collision, where low energy photons are emitted Z is equal to the net ion charge. For the X-ray region the contribution from the minimum impact parameter collisions is predominant and it is possible to assume that the screening depends on the de Broglie wavelength $\lambda_\varepsilon$ of the incident electron. If $\lambda_\varepsilon$ is smaller than the radius of the K-shell then $Z=Z_N$, if it is between the radius of the K-shell and the L-shell then $Z=Z_N-2$ and so on.

The expression for the emission power spectrum can be easily deduced from the cross section and is given by:

$$\left(\frac{dW}{dh\nu}\right)_{BR} = \frac{16}{3}\frac{\pi}{\sqrt{3}}\left(\frac{e^2}{\hbar c}\right)^3 \left(\sum_z n_z Z^2\right)\frac{\hbar^2}{m^{3/2}}\int_{h\nu}^{\infty}\frac{g_{ff}(\varepsilon,h\nu)f(\varepsilon)}{\sqrt{2\varepsilon}}\,d\varepsilon$$

where $n_z$ is the total density of ions with effective charge Z.

This formula shows that in principle the electron distribution function $f(\varepsilon)$ could be deduced from a measurement of the bremsstrahlung spectrum. In practice however this is only possible when the recombination contribution is negligible, as we will show later. When this is not the case it is customary to assume that the electrons are at the thermal equilibrium so that their energy distribution is well described by a maxwellian function

$$f(\varepsilon) = \frac{2n_e \varepsilon^{1/2}}{\pi^{1/2}(kT_e)^{3/2}} \exp(-\varepsilon/kT_e)$$

where $n_e$ is the electron density, $T_e$ the electron temperature, and the expression for the power spectrum becomes:

$$\left(\frac{dW}{dh\nu}\right)_{BR} = \frac{32}{3\sqrt{3}}\left(\frac{\pi}{2}\right)^{1/2}\left(\frac{e^2}{\hbar c}\right)^3\left(\frac{\hbar^2}{m^{3/2}}\right) n_e\left(\sum_z n_z Z^2\right)\frac{\overline{g_{ff}(kT_e, h\nu)}}{(kT_e)^{1/2}} \cdot \exp(-h\nu/kT_e) =$$

$$= 3.10^{-15}\, n_e\left(\sum_z n_z Z^2\right)\frac{\overline{g_{ff}(kT_e, h\nu)}}{(kT_e)^{1/2}}\exp(-h\nu/kT_e)\, cm^{-3}\, sec^{-1}$$

where $kT_e$ is expressed in keV and $\overline{g_{ff}(kT_e h\nu)}$, the Gaunt factor averaged over a maxwellian distribution, can be assumed equal to 1 as discussed in [7].

From these expressions we can conclude that the bremsstrahlung continuous emission from a plasma allows the measurement of the electron temperature from the exponential decay of the spectral intensity. The absolute intensity of the spectrum is influenced by the presence

of impurities which however also greatly enhance the competing process of electron recombination.

The recombination spectrum is emitted by free electrons captured in a bound state of hydrogen or impurity ion. In this event a photon is emitted whose energy is given by

$$h\nu = \varepsilon + \chi_n$$

where $\varepsilon$ is the electron kinetic energy and $\chi_n$ the binding energy of the recombination level. A continuous power spectrum is generated which reflects the shape of the electron distribution function

$$\left(\frac{dW}{dh\nu}\right)_{REC} = \sigma_r(\varepsilon,n,Z)\, h\nu\sqrt{\frac{2\varepsilon}{m}}\, f(\varepsilon)$$

A peculiar feature of the recombination spectrum is the presence of step discontinuities at photon energy corresponding to the ionization potential of the levels of the impurities present in the plasma. It is also worth noting the different dependence of the recombination and bremsstrahlung spectrum upon the electron distribution function which makes it impossible in general to obtain detailed information on $f(\varepsilon)$ from low energy X-ray measurements.

The radiative recombination cross section $\sigma_r(\varepsilon,n,Z)$ can be deduced from the better studied photoionization cross section through the detailed balance principle, the two processes being the inverse of each other. This cross section is well-known for hydrogen-like ions [8] from which we obtain

$$\sigma_r(\varepsilon,n,Z) = \frac{8\pi}{3\sqrt{3}} \frac{Z^2 e^6}{\hbar c^3 m} \frac{\chi(Z,n)}{\varepsilon} \frac{g(n)}{n^3} \frac{g_{fb}(\varepsilon,n,Z)}{h\nu}$$

where

$$\chi(Z,n) = \chi_H Z^2/n^2 = 13.6\ Z^2/n^2 (ev)$$

$g(n) = 2n^2$ is the statistical weight of the recombined level and $g_{fb}(\varepsilon,n,Z)$ is the Gaunt factor for the free-bound transition [7].

Calculations for other types of ions have been performed only in a limited number of cases and are too lengthy for an extensive use in plasma diagnostics [9].

A simple approximation is then adopted for these ions [3]:

- The recombination on the excited levels is computed in the hydrogen-like approximation with Z equal to the net ion charge.
- For the recombination on the fundamental shell the hydrogen-like formula is modified by substituting $\chi(Z,n)$ with the first ionization potential $\chi_i$ and the statistical weight with the number of unfilled states $\xi$.

With these approximations the recombination spectrum emitted by a maxwellian plasma with a density $n_z$ of impurities of nuclei charge Z is given by

$$\left(\frac{dW}{dh\nu}\right)_{REC} = 3\ 10^{-15} n_e n_z \frac{\exp(-h\nu/kT_e)}{(kT_e)^{1/2}} \cdot$$

$$\cdot\left\{\sum_i \frac{n_{z_i}}{n_z} Z_i^2 \left[\frac{\xi}{n^3} \frac{\chi_i}{kT_e} \exp(\chi_i/kT_e) + \sum_{m>n} \frac{2\chi_H Z_i^2}{kT_e m^3} \exp\left(\frac{Z_i \chi_H}{kT_e m^3}\right)\right]\right\}$$

where n is the principal quantum number of the fundamental shell and the averaged Gaunt factor has been assumed equal to the unit, see [3].

This expression is only valid for $h\nu > \chi_i$; for lower photon energies the sum for each ionization stage should be only extended over quantum states whose binding energy is lower than $h\nu$. This describes the appearance of characteristic recombination steps in the spectrum.

Between these steps the expression given shows that the spectral shape is identical to the bremsstrahlung emission, whatever the impurity and the recombination level, and the plasma electron temperature can be deduced from the experimental data. This technique is widely adopted in plasma diagnostic with different levels of complexity to obtain time and space resolved measurements [10,11].

It is evident from the previous discussion that the absolute intensity of the continuous spectrum depends on the impurity content in the plasma and on the fractional abundances $n_{zi}/n_z$ of the various ionization stages. The presence of medium Z impurities can be detected through the measurements of their characteristic $K_\alpha$ line: these impurities are mainly released in the interaction of the plasma with the vacuum chamber wall or with the limiter used to determine the radial dimensions of the discharge.

However a good estimate of the excitation rate coefficients for such lines requires extensive atomic physics calculation and the detailed knowledge of the ionization equilibrium in the plasma. Reliable data are only available for a few impurities [12] under the assumption that

corona equilibrium describes the ionization balance in the plasma.

Once the medium Z impurity densities have been estimated from their $K_\alpha$ line brightness the absolute intensity of the continuous emission can be used to evaluate the low Z impurity concentration in the plasma [10,11]. This procedure is not accurate because of the large uncertainties in the atomic physics data and in the ionization equlibrium. However it has proven to be very useful in establishing trends in the impurity behaviour with plasma parameters.

A better knowledge of impurity content in the plasma can be obtained by high resolution spectroscopy, where the lines from the different ionization stages can be identified, see below.

Good quality, low resolution spectra in the soft X-ray region (1.0÷20 keV) are obtained by means of Si--Li proportional detectors. In a typical apparatus the detector is combined with an X-ray collimator to define the field of view and the counting rate at the detector, and a thin foil absorber (usually Be or Aℓ) which cuts off the low energy part of the spectrum and define the spectral range under examination.

The main problem with this kind of set-up is due to spectral distorsions caused by pulse pile-up which, due to the exponential shape of the true spectrum, are very effective even at very low counting rates [13,14]. The use of pile-up rejecting electronics allows a counting rate not in excess of 40 kHz approximatively.

A higher counting rate and better coverage of the interesting spectral region can be obtained through the

use of multidiode detectors [10]. In this case each diode is equipped with a different filter and a different collimator to measure distortion free spectra in different spectra intervals. A complete spectrum can be obtained by matching together the different measurements. In this way a fairly complete coverage of the soft X-ray spectral region is obtained with a time resolution of some tens of milliseconds, although with a complex and costly apparatus.

## 3. X-RAY INTENSITY MEASUREMENTS

Fast measurements of X-ray emssion by the plasma can be obtained when only the low energy cut-off of an absorber filter is maintained and the X-ray flux is detected by a PIN or surface barrier photodiode. Currents in the range 0.1 - 10 μA are easily generated allowing good signal to noise ratio with a bandwidth of up to 500 kHz. Arrays of similar diodes can be used in a pin-hole camera to study the plasma emission locally.

The plasma electron temperature can be determined by the two-filter technique [15]: it is easy to show that, in the absence of line radiation and recombination steps, the ratio of the emission intensity after two absorber foils of different thickness is only a function of the electron temperature. The difficulties with this method is that independent information on the impurity density is needed so as to assess its influence on the measurement. However very fast time scale information can be produced [16].

Soft X-ray diode arrays have been used extensively in tokamak research in connection with studies of the space structure of magnetic surfaces [17]. In fact all the quantities determining the local emissivity are constant along such surfaces due to the high conductivity of the plasma along the magnetic field.

Time fluctuations of the emissivity can also be studied to reveal intrinsic fluctuation of plasma parameters or localized deformation of the magnetic surface, due to magnetohydrodynamic instabilities, which rotate with the plasma in the poloidal or toroidal direction.

The most important result obtained with this technique was the discovery of the internal relaxation mode which causes the periodical sawtooth oscillation of the electron temperature in the plasma center, Fig.2. [18]. This is the consequence of the inverse dependence of plasma electrical resistivity upon the electron temperature which makes the current density profile peaked in the center. When the plasma current is sufficiently high, the safety factor q(0) in the plasma center (q(0) is inversely proportional to the central current density) can become lower than unit and a MHD perturbation grows rapidly to final stage when a reconnection of magnetic field line within the radius at which q=1 takes place [19]. This leads to a flattening of both the current density and electron temperature profile within this region and the process starts again on a time scale which is dominated by the local power input and the plasma resistivity and heat conductivity.

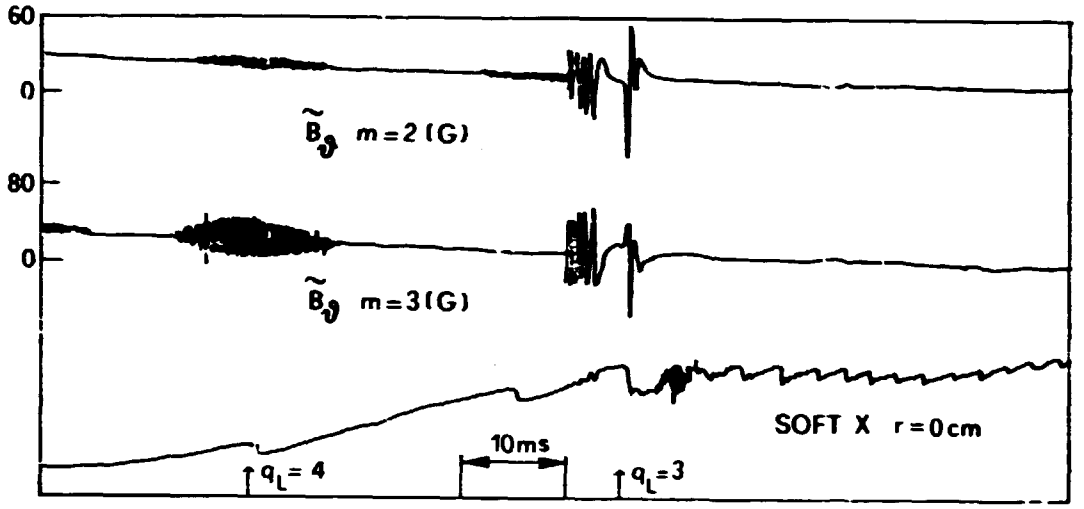


Fig. 2 Time evolution of soft X-ray intensity during the start up of a high current discharge in FT. The upper signal shows the fluctuation of two poloidal components of the poloidal magnetic field associated to the plasma current. The typical sawtooth oscillation begins when the q=3 at the plasma surface is crossed.

The study of the propagation outside the q=1 surface of the heat pulse generated during the internal reconnection offers the opportunity to determine the plasma heat conductivity [20]. Measurements carried out on various devices have shown that the propagation is diffusive and have deduced a value for the diffusion coefficient from a measurement of the time to peak. When compared to the thermal diffusivity inferred from the thermal balance in the discharge, this method seems to give reliable results [20].

The heat pulse propagation technique can also be applied in the absence of internal relaxation by inducing the heat pulse with a localized deposition of additional heating in the plasma [21].

A great deal of work in soft X-ray imaging of tokamak plasmas has been performed to study magnetohydrodynamic perturbations and the related phenomenon of plasma disruption [17]. The presence of MHD perturbation on the structure of magnetic surfaces is generally revealed by time periodic oscillation in the X-ray signals. These oscillations are thought to be due to helical deformation of the magnetic structure, the plasma rotation translating the spatially periodical structure into a time oscillating signal.

The principles of tomographic reconstruction have to be used in these conditions, the cylindrical symmetry of the magnetic surfaces being lost during these phenomena. Basically two techniques have been applied:

- When the plasma rotation can be assumed to be rigid, the mode spatial structure can be deduced from line integral measurements obtained with one array in a way similar to rotating the patient in front of a tomographic scanner [22].
- When the rotation is not rigid or the mode evolution is faster than the rotation period, many angular views are necessary. Then the maximum poloidal harmonic detectable is roughly given by the number of arrays [23,24,25,26].

## 4. HIGH RESOLUTION SPECTROSCOPY

In recent years high resolution X-ray spectroscopy of tokamak plasmas has gained increasing importance as a consequence of the steady increase of electron temperature achieved with the application of additional heating methods. In fact when the plasma temperature reaches the multi keV range, metallic impurity atoms extracted from the walls of the vacuum chamber are present in the plasma core in the He-like and H-like ionization stage and radiate characteristic spectra around their $K_\alpha$ transition. At nuclear charge value around 25, these spectra lie in the 1-5 Å spectral region and are rich in satellite lines located at the long wavelength side of the main optically allowed line.

In fact for high Z, highly stripped ions, in a hot plasma, besides the usual electron impact process, two other mechanisms of line formation become effective, namely the dielectronic recombination of free electrons and the collisional excitation of inner-shell electrons, both

leading to the emission of satellite lines only slightly displaced in wavelength from the main optically allowed line [27]. In this situation, besides the line shapes from which the plasma ion temperature can be inferred [28], it is easy to measure line-intensity ratios accurately; in fact, owing to the small spectral separation of the lines, the relative calibration of the experimental apparatus at different wavelengths is not needed. These ratios have important applications in plasma diagnostic because the different excitation mechanisms of the lines imply a different dependence of the line intensities from plasma parameters [27].

A considerable amount of the theoretical [29,30,31, 32] and experimental [33,34,35,36,37,38] work has been carried out on this subject owing to the importance of this diagnostic method for both laboratory and astrophysical plasmas. Here a short description of the basic principle is given and, as examples, results obtained from the FT tokamak will be presented.

A typical spectrum around the $2p \rightarrow 1s$ transition in He-like iron is shown in Fig.3. The data have been obtained by means of a crystal spectrometer in the Johann configuration [38] whose principle of operation is illustrated in Fig.4: X-rays of different wavelength are focussed at different points, in accordance with Bragg's law, along the Rowland circle tangent to the cylindrically curved crystal at its center and having twice its curvature. On the other hand, the crystal diffracts X-rays of different wavelength passing through point-like sources located at different places on the same cirlce. It follows that an instrument using this optical scheme and a posi-

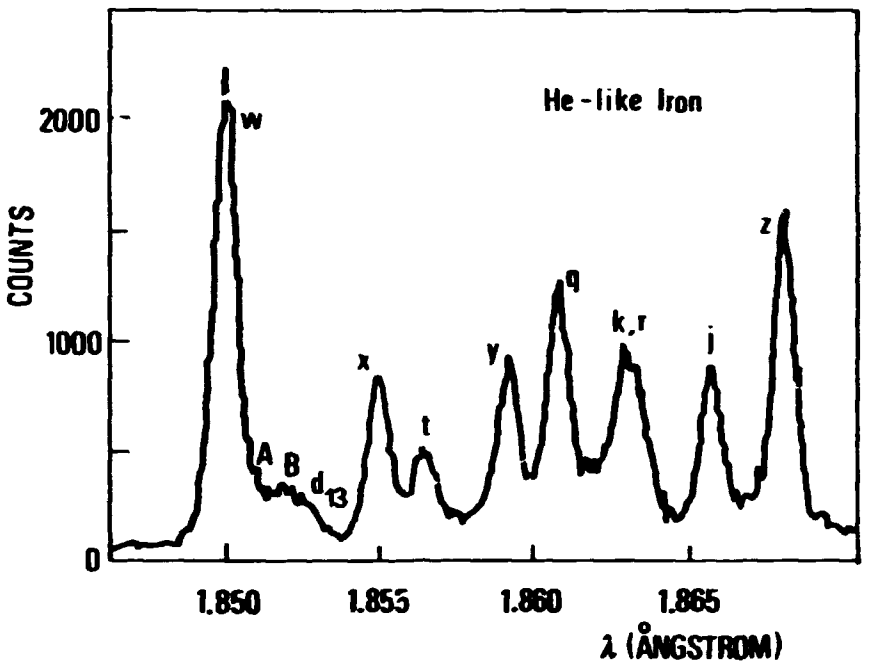


Fig. 3 High resolution X-ray spectrum from He-like iron in FT. The labelling of emission lines is described in [27].

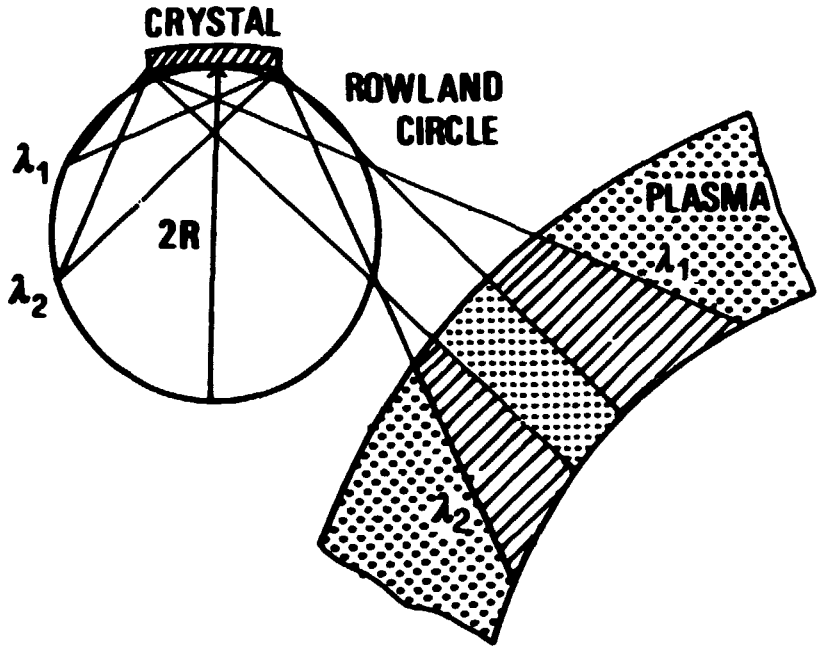


Fig. 4 Optical scheme of the Johann mounting.

tion sensitive detector is a true polychromator but needs a homogeneous extended source. This is not really a drawback for a source symmetrical along a direction such as a tokamak plasma [39].

Spectral resolving power around 20000 is necessary in order to study in detail line shapes and it can be obtained by using resolving crystals, usually quartz cut parallel to different planes depending on the wavelength range to be observed, and long curvature radius, around a few meters. Multiwire proportional chambers are used as position sensitive detectors since they offer good space resolution and large detection area.

Only some of the lines shown in Fig.3 are characteristic of a He-like configuration. The analysis of the energy level diagram of the first excited level of a He-like ion shows that only four lines can be emitted by radiative transition from one of these levels to the ground state:

- the resonance line w
  $1s2p(^1P_1) \rightarrow 1s^2(^1S_0)$
  (electric dipole transition)
- two intercombination lines x
  $1s2p(^3P_2) \rightarrow 1s^2(^1S_0)$
  (magnetic quadrupole transition)
- and y
  $1s2p(^3P_1) \rightarrow 1s^2(^1S_0)$
  (electric dipole transition)
- the forbidden line z
  $1s2s(^3S_1) \rightarrow 1s^2(^1S_0)$
  (relativistic magnetic dipole transition)

Of the remaining two states, the $1s2s(^1S_0)$ only decays to the ground state through a two photon transition, whereas the $1s2p\ (^3P_0)$ decays radiatively into the $1s2s(^3S_1)$ with emission of a low energy photon.

Rate equations can be written for the population $N_j$ of these levels and in the steady state we have

$$N_j\Big(\sum_{i<j} A_{ji}^{(r)} + N_e \sum_k C_{jk}\Big) = \sum_{i<j} N_i A_{ij}^{(r)} + N_e \sum_k N_k C_{kj} \quad ,$$

where $N_e$ is the electron density, $A_{ij}^{(r)}$ the radiative transition probability and $C_{ij}$ the electron collisional excitation or de-excitation rate for the $|i> \rightarrow |j>$ transition.

The influence of the electron density on the ratio between level population is only important when collisional processes have a probability comparable to the radiative ones. This has important application for the diagnostic of astrophysical plasmas [40], but in tokamaks the electron density is often low enough that all the collisional processes, except the excitation from the ground state, can be neglected.

Detailed calculations of line intensities have been produced for a variety of He-like ions [29,31,35], including the effects of radiative cascades from highly excited states. Here we consider only the w line for which the radiative transition probability to the ground state is much higher than the radiative transition probability to any excited state. In these conditions the line intensity $I_w$ is given by

$$I_w = N_e N_{He} C_R(T_e) \quad ,$$

where $N_{He}$ is the density of the He-like ions and $C_R(T_e)$ is the effective excitation rate, i.e. the average of the transition cross section over a maxwellian distribution function. For illustrative purposes we use here a simple approximation for $C_R(T_e)$ given by Van Regemorter [41]

$$C_R(T_e) = 3.15\times10^{-2} f \bar{g} \frac{E_H}{E_0} \left(\frac{E_H}{kT_e}\right)^{1/2} \exp(-E_0/kT_e) \quad cm^3 sec^{-1}$$

where f is the transition optical oscillator strength, $\bar{g}\simeq 0.2$, $E_H$ is the Rydberg value, $E_0$ the transition energy and $T_e$ the plasma electron temperature.

Besides the four lines we have discussed, the rest of the lines in Fig.3 are emitted by ions in a Li-like configuration. The most obvious mechanism for their production is the direct collisional excitation of an inner shell electron. Their intensity can be described as [27]

$$I_{IS} = Ne\, N_{Li}\, C_{IS}(T_e) \frac{A_R}{A_{tot}}$$

where $A_{tot}$ is the total decay probability of the upper level (radiative + autoionization), $A_R$ the radiative decay rate of the transition considered and $C_{IS}$ is the excitation rate coefficient which can be expressed by means of the Van Regemorter approximation.

The ratio $I_{IS}/I_w$ turns out to be slightly dependent on the electron temperature and can be used to determine $N_{Li}/N_{He}$. This information is extremely important as the impurities in a tokamak can diffuse across the magnetic surfaces and the simple corona model for the ionization equilibrium is no longer valid.

The process of inner-shell excitation cannot account for some of the lines present in the spectrum in Fig.3. It is the case of the line j and the lines A,B and $d_{13}$ which are due to transition from a double excited configuration of Li-like ions of the kind

$1s2pn\ell \rightarrow 1s^2n\ell$.

Whenever the upper state of a transition involves the excitation of two electrons, the electron impact process has a negligible probability and the line is essentially excited by dielectronic recombination when the radiation less capture of a free electron by a He-like ion takes place with a reaction of the kind

$$x_z^{Z-2}(1s^2) + e \rightarrow x_z^{Z-3}(1s2pn\ell)$$

A key feature of this phenomenon is that only electrons whose kinetic energy is equal to the energy difference $E_s$ between the Li-like excited level and the ground state of the recombining ion participate in the reaction [42]. From this point of view there is a remarkable difference with the electron impact excitation of the w line which can be performed by all the electrons having a kinetic energy greater than the transition energy $E_0$.

The involvement of different positions of the electron distribution function make it easy to understand the strong electron temperature dependence of the intensity ratio of a dielectronic satellite to the w line in a maxwellian plasma.

From a theoretical point of view the intensity of a dielectronic satellite line emitted in a transition from an excited level s to a lower level f is given by [27]

$$I_s(f) = 3.3\times10^{-24} N_e N_{He} \left(\frac{E_H}{kT_e}\right)^{3/2} \frac{g_s A_a(s) A_r(s\rightarrow f)}{A_{tot}(s)} \cdot$$

$$\cdot \exp(-E_s/kT_e) \quad cm^{-3}s^{-1}$$

where $A_a(s)$ and $A_{tot}(s)$ are, respectively, the autoionization rate and the total decay rate of the upper level, $A_r(s\rightarrow f)$ is the radiative decay rate within the channel $s\rightarrow f$ corresponding to the line considered, and $g_s$ is the statistical weight of the upper level of the transition.

When all the atomic physics parameters are accurately known. the plasma electron temperature can be derived from the intensity ratio of a dielectronic satellite to the w line. An example of results obtained in a high-density discharge in FT is shown in Fig.5: the electron temperature was obtained from n=3 dielectronic satellites to the resonance line in FeXXV with a good agreement with the Thomson scattering value and the time evolution determined by the electron cyclotron emission diagnostic.

This agreement is not expected and not found in discharge where the electron distribution is far from the thermal equilibrium. In this case the spectroscopic measurements can be exploited to obtain information on the non thermal electrons in the plasma [43].

High resolution X-ray spectroscopy also allows the determination of the ion temperature in the plasma by analyzing the line shape of the resonance line. In fact

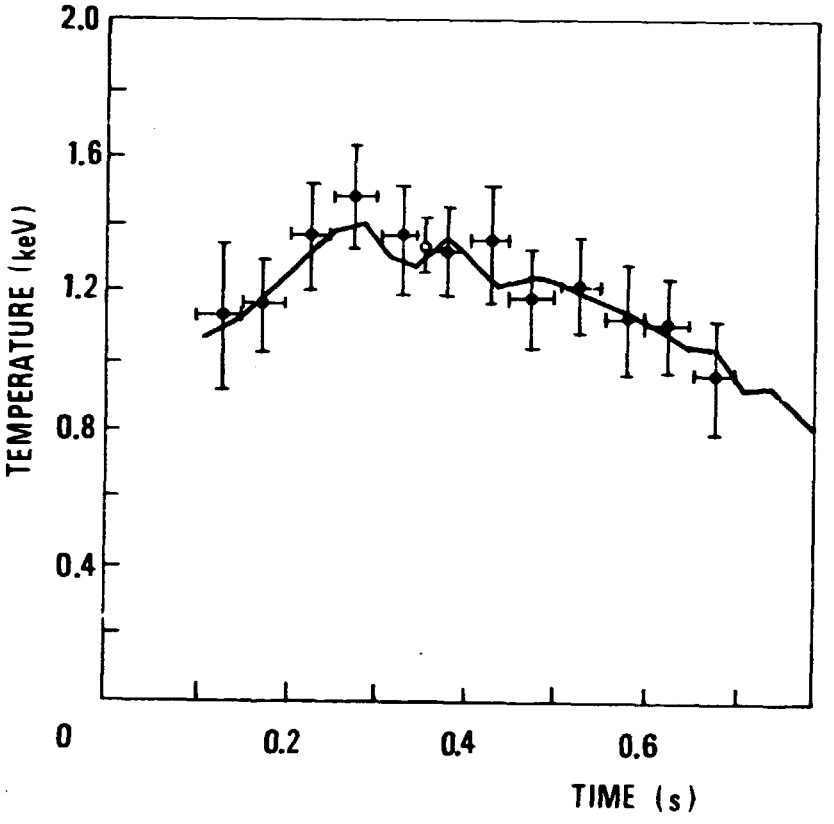


Fig. 5 The time evolution of the electron temperature measured in a high density discharge in FT by electron cyclotron emission diagnostic (continuous line) and the Thomson scattering value (open dot) are compared with data points (crosses) obtained from the line ratio of n=3 dielectronic satellites ($A, B, d_{13}$) and the resonance line w.

it turns out that their intrinsic radiative width is typically about a factor ten lower than the Doppler width and the ion temperature can be obtained by fitting a Voigt profile to the experimental data [28].

In FT we injected argon in the discharge [44] and observed the spectrum of the H-like ion: Fig.6 shows the doublet resonance lines Lyman $\alpha_1$ and $\alpha_2$ and some dielectronic satellites T and $\lambda$. The Lyman doublet was used to determine the ion temperature and the result successfully compared with the fast neutral analysis determination, Fig.7.

The diagnostic of the ion temperature by means of high resolution X-ray spectroscopy is expected to play an important role on large dimension tokamaks like JET and TFTR where the plasma is not transparent to the fast neutrals.

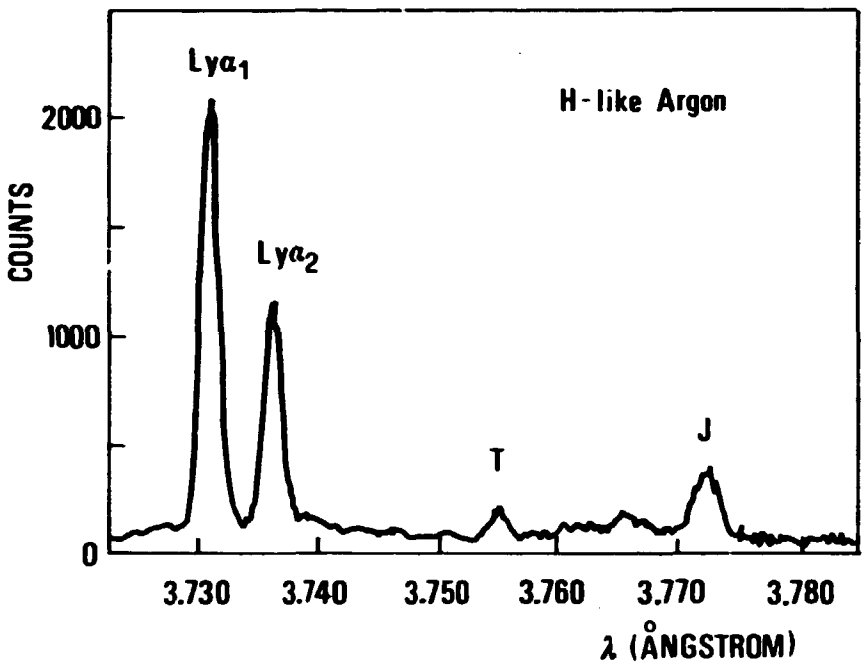


Fig. 6 Hydrogen-like argon spectrum in FT. T and J are dielectronic satellites.

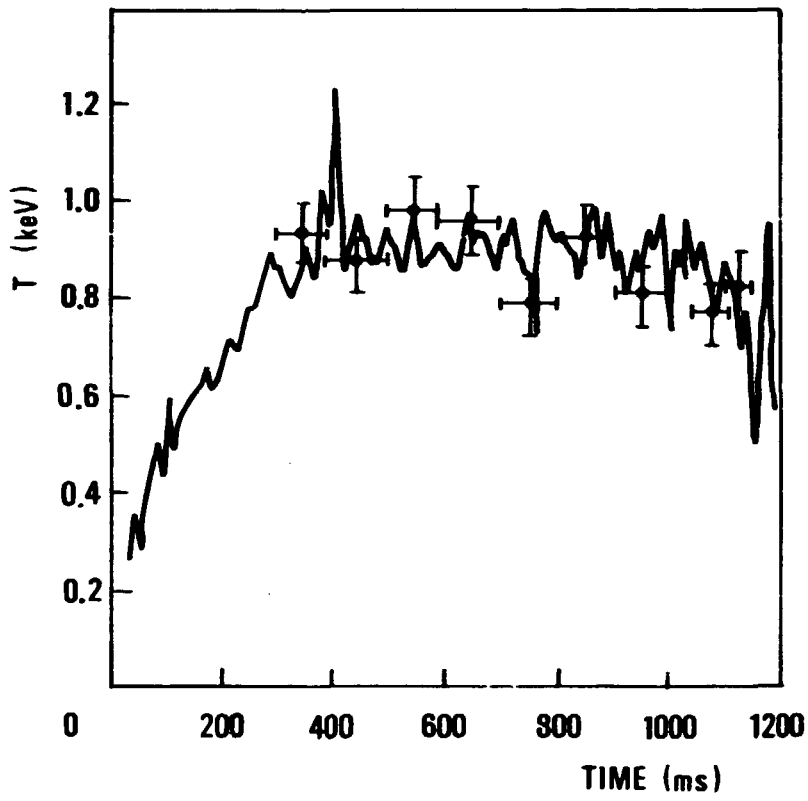


Fig. 7 Jon tempeature as a function of time for a typical FT discharge, fast neutrals (full line) and line broadening (crosses) results.

REFERENCES

[1] For an introduction to the problem of thermonuclear controlled fusion and the tokamak concept see e.g. H.P. Furth in "Fusion", ed. E. Teller, Academic Press (New York) 1981.

[2] D.A. Sheheglov, JEPT Lett. 6 (1967) 365.

[3] S. von Goeler et al., Nucl. Fus. 15 (1975) 301.

[4] S. von Goeler in "Diagnostic for Fusion Experiments", eds. E. Sindoni and C. Wharton (Pergamon Press, Oxford, 1979).

[5] J.E. Rice et al., Phys. Rev. A25 (1982) 1645.

[6] A.J.K. Sommerfeld, Atombau und Spektrallinien (Ungar New York 1953) vol.2, ch. 7.

[7] W.J. Karzas and R. Latter, Astrophys. J. Suppl. 55 (1961) 167.

[8] J.A. Gaunt, Philos. Trans. R. Soc. Lond. A229 (1930) 163.

[9] Young Soon Kim and R.H. Pratt, Phys. Rev. A27 (1983) 2913.

[10] E.H. Silver et al., Rev. Sci. Instrum. 53 (1982) 1198.

[11] R. Bartiromo and A. Tuccillo, Nuovo Cimento 633 (1981) 696.

[12] A.L. Merts, R.D. Cowan and N.H. Magee, Los Alamos Report LA-G220-MS (1976).

[13] R. Bartiromo et al., Report CNEN 80.46, Associazione Euratom-CNEN sulla Fusione, Centro di Frascati, Frascati, Rome, Italy (1980).

[14] F.H. Tenney, Princeton Plasma Physics Laboratory Report, PPPL-1999 (1983).

[15] F.C. Jahoda et al., Phys. Rev. 119 (1960) 843.

[16] J. Kiraly et al., Rev. Sci. Instrum. 56 (1985) 827.

[17] N.R. Sauthoff et al., Nucl. Fusion 18 (1978) 1445.

[18] S. von Goeler et al., Phys. Rev. Lett. 33 (1974) 1201.

[19] B.B. Kadomtsev, Sov. J. Plasma Phys. 1 (1975) 389.

[20] M. Soler and J.D. Callen, Nucl. Fusion 19 (1979) 703.

[21] G.J. Jahns et al., General Atomic Technologies Report GA-A17858, San Diego, California (1985).

[22] N.R. Sauthoff and S. von Goeler, IEEE Trans. Plasma Sci. PS7 (1980) 141.

[23] P. Smeulders, Max-Planck-Institut für Plasmaphysik, Report IPP2/252, Garching bei Munchen (1981).

[24] A.P. Navarro et al., Rev. Sci. Instrum. 52 (1981) 1634.

[25] E. Silver and W. Roney, IEEE Trans. Plasma Sci. P58 (1980) 231.

[26] R.S. Granetz and J.F. Camacho, Nucl. Fusion 25 (1985) 727.

[27] J. Dubau and S. Volonté, Rep. Prog. Phys. 43 (1980) 199.

[28] M. Bitter et al., Phys. Rev. Lett. 42 (1979) 304.

[29] F. Bely-Dubau et al., Mon. Not. R. Astron. Soc. 198 (1982) 239.

[30] F. Bely-Dubau et al., Mon. Not. R. Astron. Soc. 186 (1979) 405.

[31] F. Bely-Dubau et al., Mon. Not. R. Astron. Soc. 201 (1982) 1155.

[32] L.A. Vainshtein and V.I. Safronova, At. Data Nucl. Data Tables 21 (1978) 49.

[33] M. Bitter et al., Phys. Rev. Lett. 43 (1979) 129.

[34] TFR Group et al., J. Phys. B15 (1982) 1007.

[35] F. Bely-Dubau et al., Phys. Rev. A26 (1982) 3459.

[36] E. Kallne et al., Phys. Rev. Lett. 49 (1982) 330.

[37] M.L. Apicella et al., Phys. Lett. 98A (1983) 174.

[38] R. Bartiromo et al., Nucl. Instrum. Methods 225 (1984) 378.

[39] K.W. Hill et al., Phys. Rev. A19 (1979) 1770.

[40] A.H. Gabriel and C. Jordan in: Case Studies in Atomic Collision Physics, eds., E.W.McDaniel and M.R.C. McDowell (North Holland, Amsterdam, 1972) vol. 2.

[41] H. Van Regemorter, Astrophys. J. 136 (1962) 906.

[42] A.H. Gabriel and K.J.H. Phillips, Mon. Not. R. Astron. Soc. 189 (1979) 319.

[43] R. Bartiromo et al., Phys. Rev. A32 (1985) 531.

[44] R. Bartiromo et al., Nucl. Instrum. Methods B9 (1985) 679.

# LOW ENERGY ELECTRON BEAMS GENERATOR FOR IRRADIATION TESTS

Eugenio Fiorentino*, Italo Giabbai, Gualtiero Giordano, Tommaso Letardi, Angelo Marino*

ENEA, Dip. TIB., Divisione Fisica Applicata, CRE, Frascati, C.P. 65, 00044 Frascati, Rome, Italy.

ABSTRACT

A low energy electron beam generator is described. The system has operated at an electron energy of 200 keV, with a peak current density of more than 100 A/cm$^2$. Future developments are also presented.

(*) Dip. TIB., Casaccia

## 1. INTRODUCTION

Low energy (l.e.) electron beams are actually finding an ever increasing variety of applications as irradiation sources. Electron beam generators of relatively low energy (lower than 1 MeV) and high current (up to a few tens of kA) have been developed recently for many industrial and research applications like laser pumping, metal welding etc. A great interest is now growing also for irradiation and sterilization applications. The main advantage of a l.e. electron beam generator lies in the fact that it does not need heavy shieldings as those required by γ-ray sterilizers at the same irradiation dose. L.e. electrons are indeed easily absorbed by a lower thickness of material than γ-rays. On the other hand their use is convenient only for the irradiation of material of a few tens of centimeters thickness because the electron energy increases with the thickness of irradiated material.

Other advantages are the higher dose rate attainable, so that larger amounts of material per unit time can be irradiated, and the easier, and hence more reliable, monitoring of the working parameters of the irradiation facility.

Finally electron beams can be easily scanned over wider areas by suitable magnetic field whereas this feature is absolutely unavailable when using a γ-ray sterilizer.

The ENEA-TIB electron beam generator, installed at the Frascati Centre, has been developed in the frame of the Rare Gas Halide research program, but has been recently properly modified in order to carry out some irradiation tests aimed at packages sterilization.

## 2. SYSTEM DESCRIPTION

The whole system can be schematically represented as shown in Fig.1. A CONTROL CIRCUIT provides the proper timing for the spark gaps and allows adjustment of the operating repetition frequency. A variable HIGH VOLTAGE POWER SUPPLY is used to charge the primary capacitor (see below) and to vary the beam energy while the HIGH VOLTAGE PULSERS are used to drive the spark gaps. Finally a monitor circuit allows control of the correct runnning of the accelerator: it can be a simple oscilloscope and/or a data acquisition system. Compressed dry air is used in the spark gaps and a vacuum pump is necessary for the diode.

The electron beam generator consists of a voltage multiplier, based on a resonant transformer, and a cold cathode vacuum diode. The equivalent electric circuit is illustrated in Fig.2. $L_1$, and $L_2$ are the primary and secondary inductances of the transformer windings, k is the transformer coupling coefficient. $C_1$ is a real capacitor and the energy stored in it is resonantly coupled to a pulse forming line whose capacity is $C_2$. The electron beam pulse duration is determined by the pulse forming line. When spark gap 1 is fired, capacitor $C_1$ is discharged through $L_1$ and the voltage across $C_2$ varies resonantly as in Fig.3. If SG2 is fixed when the voltage across $C_2$ has a maximum, the cathode of the diode is pulsed and an electron pulse is obtained towards the anode. If this is a very thin foil of metal, the electrons cross it and a pulsed electron beam is available.

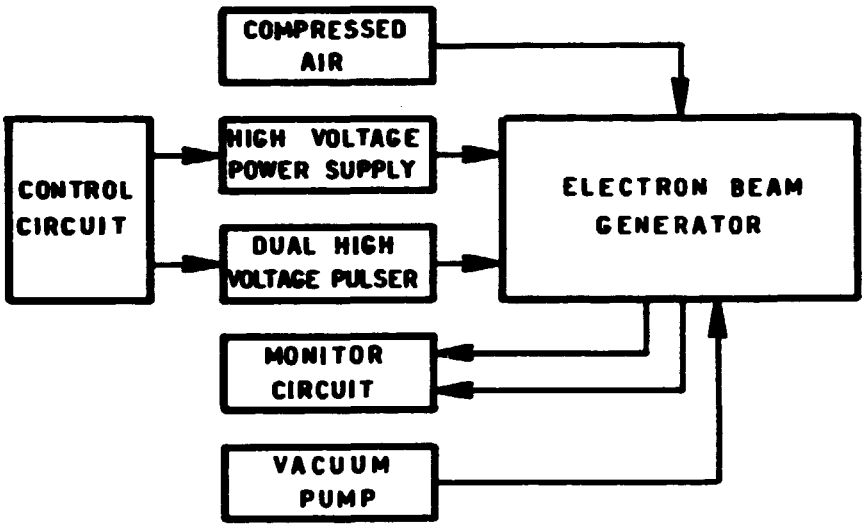


Fig.1 Block diagram of the electron beam generator

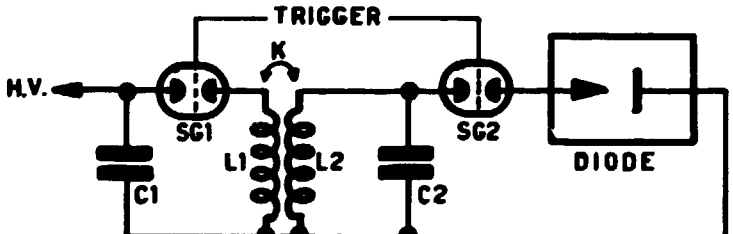


| | | |
|---|---|---|
| C1 | 450 | nF |
| C2 | 1 | nF |
| L1 | 100 | nH |
| L2 | 32 | μH |
| K (transformer coupling coefficient) | 0.6 | |
| G=Vout/Vin | 13.5 | |

Fig.2 Equivalent electrical circuit.

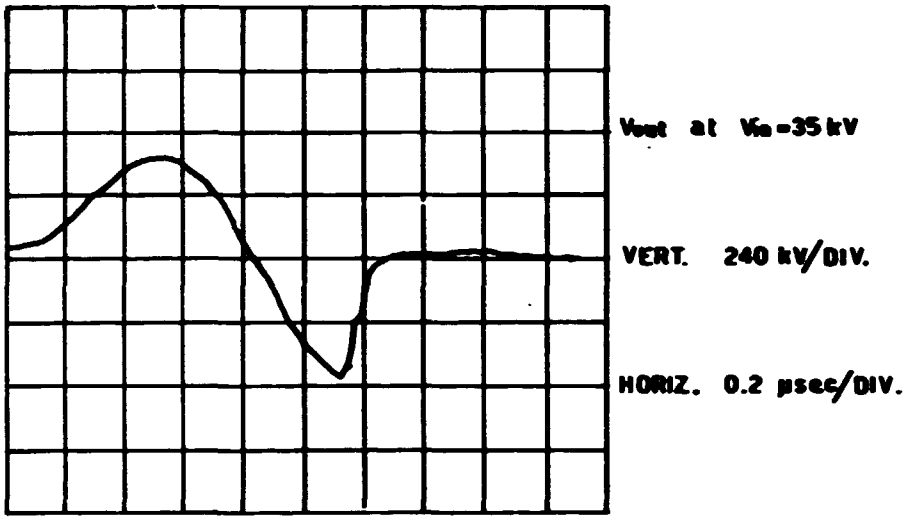


Fig.3 Voltage waveform on the secondary capacitor.

In the actual configuration the multiplying factor due to the resonant transformer is 13.5 so that at a maximum primary voltage of 35 kV, a secondary voltage of 480 kW is obtained and the electron beam energy is E=220 keV.

The cathode is a graphite rod whose area is 10x120 $mm^2$ while the anode is a Ti foil 25 μm thin.

The diode voltage and current picked up by suitable probes are used to continuously monitor the accelerator performances. Typical monitor signals are shown in Fig.4.

Other performances of the electron beam generator have been measured, i.e. beam uniformity and dose per pulse.

The beam uniformity has been evaluated exposing a green cellophane foil to the radiation emitted. The cellophane transparency increases proportionally to the absorbed radiation and a measure of it in the exposed part directly shows the beam uniformity. From Fig. 5 it is possible to verify that the beam uniformity, over the cathode length of 120 mm, is better than 10%.

The dose per pulse supplied by the electron beam generator has been evaluated with a calorimetric method, i.e. measuring the temperature increase of an aluminium sheet (100 μm thin) due to the energy loss in it by the electron beam. The does per pulse resulted to be 1 Mrad/pulse.

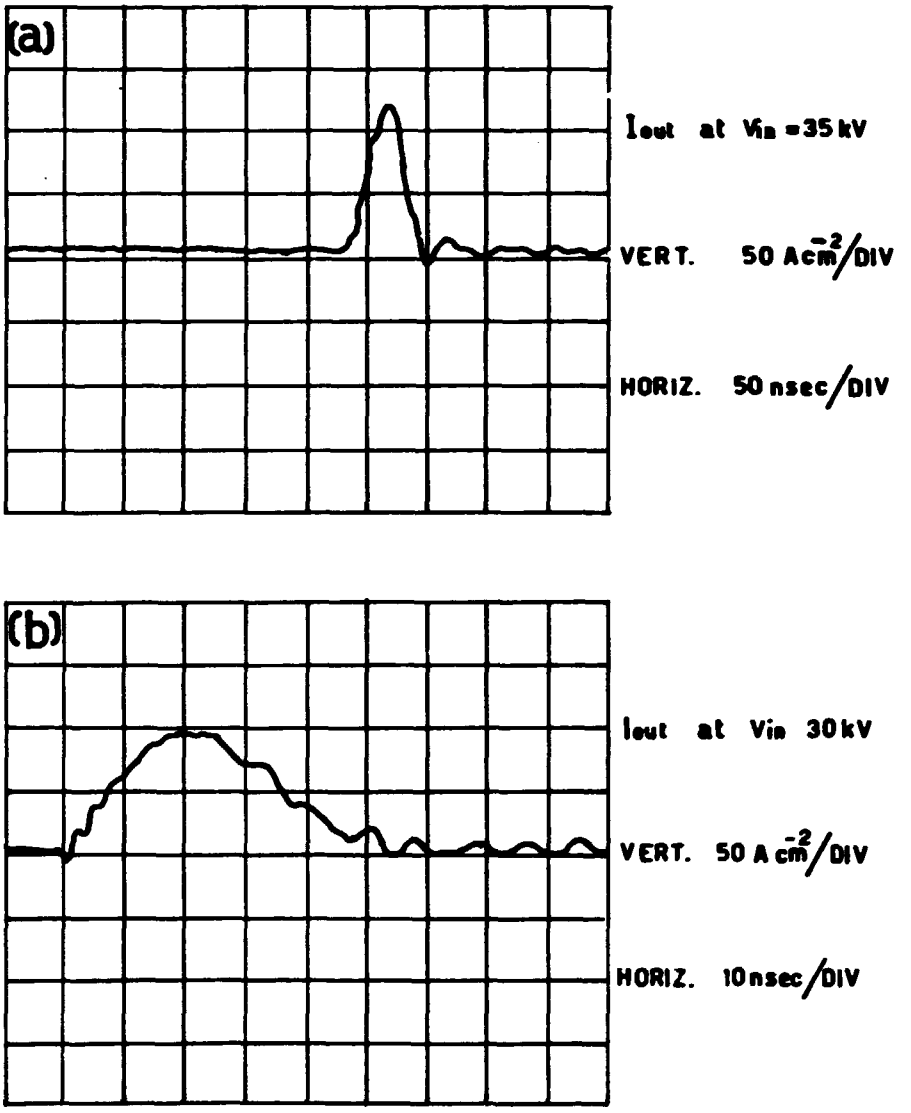


Fig.4 Output current.

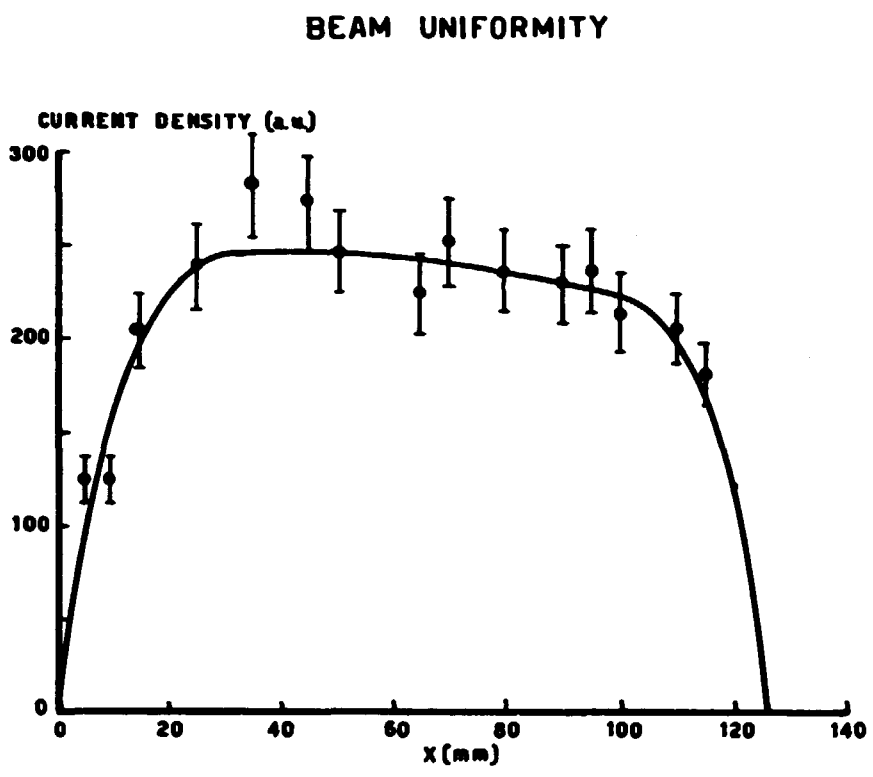


Fig.5 Beam uniformity as measured with blue cellophane disometry.

Finally the beam energy has been evaluated comparing the measured dose in cellophane vs. depth with the theoretical expected values for various beam energies (Fig.6). The agreement of the experimental data with the theoretical curve corresponding to 200 keV electrons is clearly shown.

Figs 7 a) and b) respectively show the electron beam generator and its exploded schematic view.

The apparatus has been operated reliably up to 8 Hz repetition frequency in the burst mode and a higher frequency version is under development.

## 3. CONCLUSION

The resonant transformer electron beam generator resulted to be a useful and reliable tool. The apparatus is modular and, only changing a few parts, it is possible to obtain modified performances. Namely, for excimer laser pumping, other versions have been realized at higher energy (up to ~400 keV) or higher current (up to 20 kA) or with wider pulse duration (up to 250 msec). Electron beam dimensions can also be varied modifying the diode design and a version has been built with a beam are of 40x800 $mm^2$. The same system, operated with an internal tungsten target, can deliver X ray beams of high spatial uniformity.

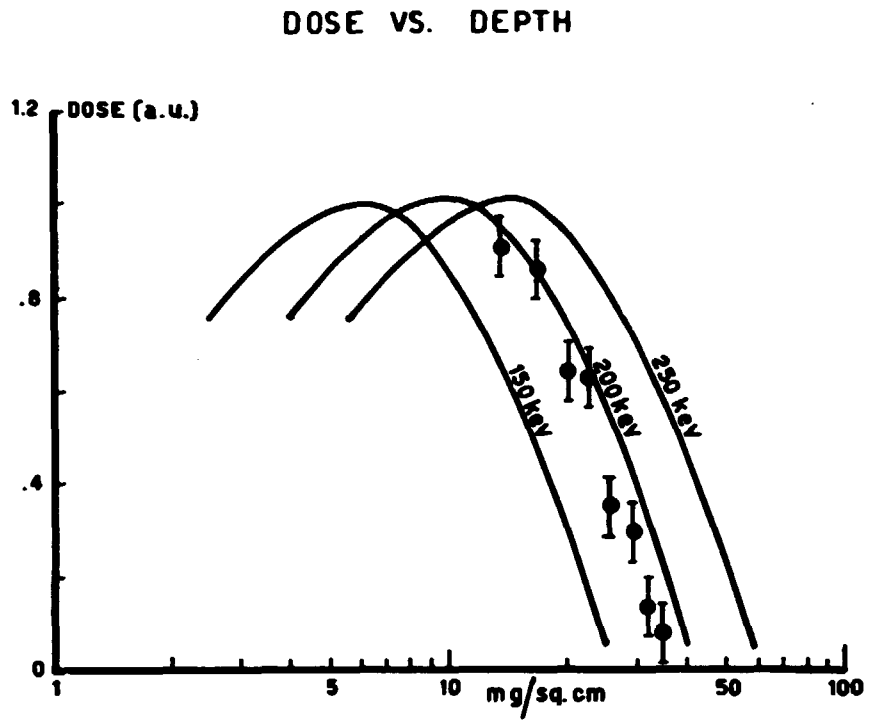


Fig.6 Dose vs. depth distribution, with calculated curves at different energies.

a

E-BEAM GENERATOR (schematic exploded view)

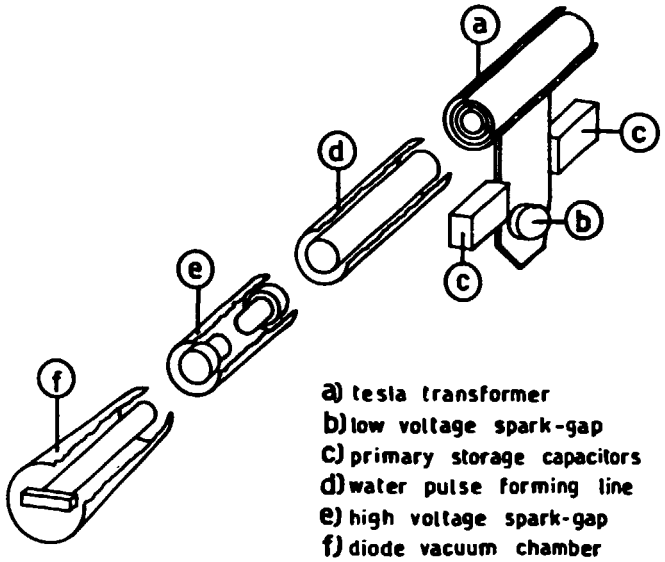


b

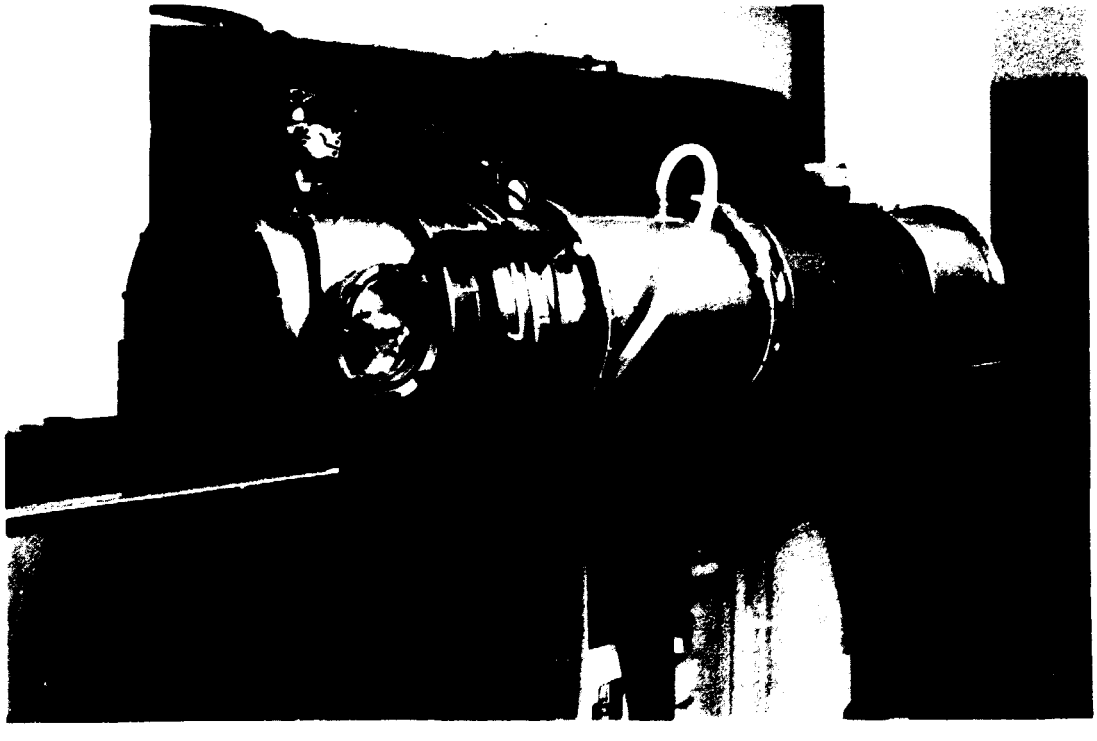

Fi.7 (a),(b) Exploded view and picture of electron beam generator.

# TIME RESOLVED NEUTRON YIELD MEASUREMENTS ON THE F.T. DEVICE

Salvatore Podda

Associazione EURATOM-ENEA sulla Fusione, Centro Ricerche Energia Frascati
C.P. 65, 00044 Frascati, Rome, Italy.

ABSTRACT

A system of four $BF_3$ proportional chambers for time resolved neutron yield measurements is operative on the F.T. (Frascati Torus) device. The detector and techniques adopted are not new, but the problems related to neutron field radiation measurements around complicated geometrical structures such as tokamak devices still remain. The determination of plasma parameters from such measurements is a completely new field of investigation subject to continuous improvements also in view of the feasible application to the control of future fusion reactors.

The absolute calibration of neutron detectors in the presence of extended neutron sources and large scattering masses, such as tokamak devices, presents a major problem. The techniques employed for $BF_3$ chambers calibration are described in this paper.

In thermonuclear plasmas the neutron yield is related to ion temperature through the density. On the F.T. device, neutron yield measurements and charge exchange analyzers are the only routine methods of monitoring ion temperature. The method and result for this measurement are reported.

We note that neutron yield measurements in fusion devices give quantative and qualitative information about ion velocity distribution and dislocation of non-thermonuclear sources. The results of neutron yield measurements in different working regimes of F.T. are presented.

## 1. Introduction

The system of four $BF_3$ proportional chambers operating on the F.T. (Frascati Torus) device (R=83.cm, a=20.cm, $B_t$=40.,60.,80.kG, $I_{pmax}$=600.kA) is used for neutron yield measurements.

The boron trifluoride proportional chambers are today a standard tool in neutron physics [1]. Largely used in fission reactors, in the last twenty years they have also become standard for tokamak devices where the problems to be tackled are original and subject to large developments. For instance, the problem of the calibration of neutron detectors has no definitive solution: in our case we made use of a technique employing "passive" neutron sources inserted at different locations in the torus, and activation techniques for source absolute calibration.

The physics which correlates the neutron field radiation to plasma conditions is another field of investigation and development. In particular, hypotheses on ion function distribution should be studied and formulated. We present some results where, assuming Maxwellian ion distribution, ion temperature can be measured, and different ion distributions can be pointed out.

In conclusion, we present the results of measurements for neutron sources other than thermonuclear ones, and evidence their properties.

## 2. The Detection System

The system is manufactured by STUDSVIK AB ATOMENERGI SWEDEN and consists of a local unit composed of the chamber tube surrounded by a shield of polyetilene and boron

plastic (mod.5210C), a preamplifier near the chamber (mod. 4614C) needed to drive long coaxial cables (≈50.m), and a remote unit with all the necessary electronics (mod. 2002B, power supply discriminator, amplifier, etc.).

The polyetilene shield has moderating and absorbing properties. The boron plastic absorbing shield reduces detector sensitivity and can be removed when maximum sensitivity is required. In this case an increase in sensitivity of 20. has been measured. We have added a copper shield against noise induced by the rapidly varying electromagnetic field due to radio frequency (R.F.) additional heating.

The discriminator setting (2.V), the bias voltage (2200.V) and the differentiation time (1 μs) of the preamplifier are those suggested by the manufacturer who claims that under such conditions 200. R/h of γ radiation results in 1.cps.

## 3. The Calibration

Because of its high magnetic field, F.T. is very compact with a limited number of accesses, so it has not been possible to insert any kind of device to move the source simulating toroidal and poloidal extension. We have placed the source in three positions only and moved the detectors along the torus therefore assuming a symmetry in the disposition of the scattering masses around the torus.

The detectors are placed (Fig.1) on a circle of 67.5 cm. radius centered on the torus center with an angle of 90° between two adjacent detectors. This disposition

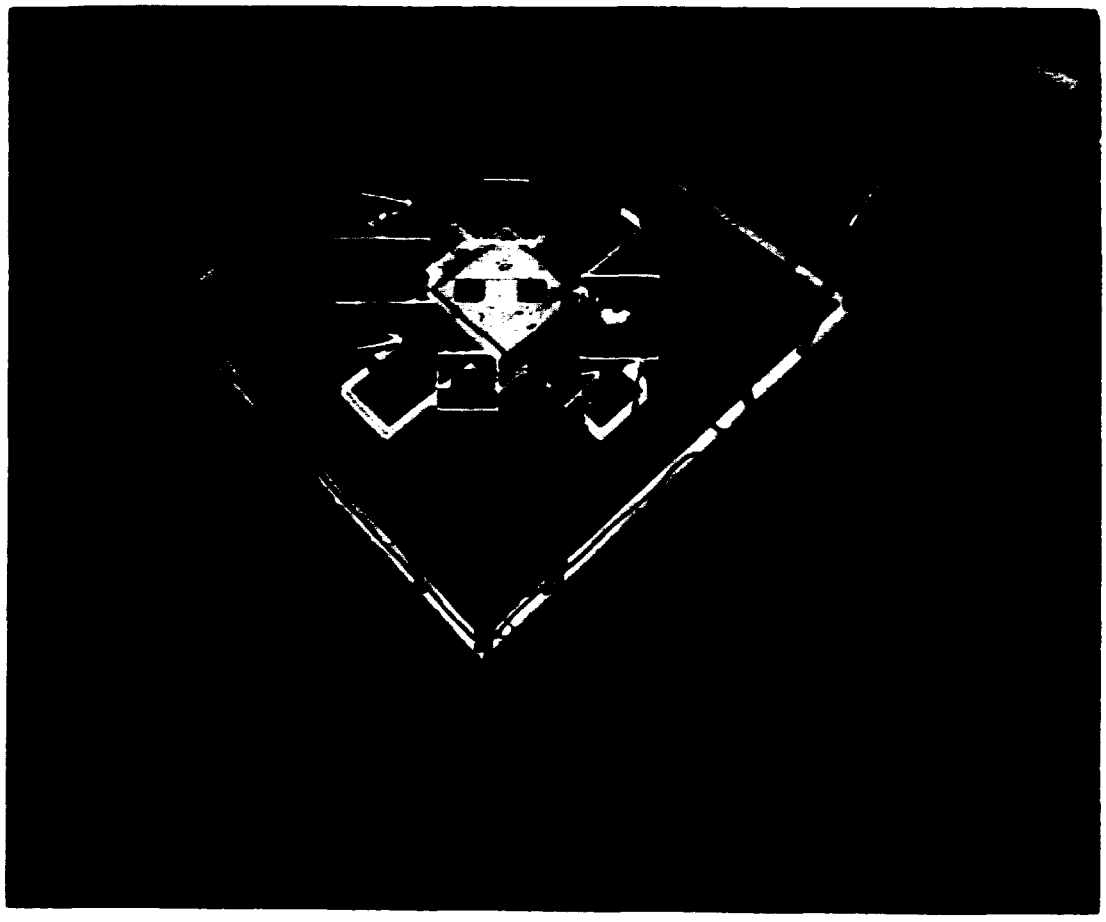

Fig. 1 Dislocation and insertion positions of detectors for calibration: circles, detectors positions (the foruth was temporarily dismounted); arrows, insertion position of AmB neutron sources for calibration.

was chosen to evidence eventual toroidal anisotropy. To prevent saturation during discharges with a high level of neutron emission, different positions at a great distance from the torus and detectors with a different absorbing shield have been calibrated.

A source (AmB) of known intensity IO ($5.10^6 sec^{-1}$) has been inserted centering on the torus axis. The measurements are taken for consecutive cycles of 90. sec. and the counting data are then fitted to a trigonometric function:

$$F(\theta) = A0 + A1 \cos(\theta-\theta0) + A2 \cos2(\theta-\theta0)$$

whose mean value on a circle is A0. The ratio between the number of emitted nuetrons during the measurement time and the mean value A0 is then taken as the calibration constant. For the three positions of insertion of the sources we obtain:

$\alpha_1 = 8.9\ 10^5$
$\alpha_2 = 9.8\ 10^5$
$\alpha_3 = 1.0\ 10^6$
$\bar{\alpha} = 9.6\ 10^5$

The evaluation of errors on this measurement is impossible. However, we note that the small deviation between values (≈10%) supports our hypothesis on symmetry in the disposition of scattering masses.

The activation technique gives a method of calibrating the detectors independently, so we have a check on

the previous method. During a set of ohmic discharges of F.T., we have inserted In samples near the plasma, which activate through the reaction:

$$In^{115}\ (n,n')\ In^{115m}$$

By decay counting we evaluate the number of neutrons seen from samples, and hypothesizing on the neutron source we obtain the absolute yield [2]. Comparing these data with the counts from the $BF_3$ chambers we obtain the calibration constants. The values are 1.9 times larger than those obtained from the other technique. We assumed the average between the two values as calibration constants and the semidispersion as errors.

## 4. The Measurements

In Figure 2 we show neutron rate and correlated ion temperature measurements obtained from a typical ohmic discharge on F.T.. This kind of discharge does not present either suprathermal behaviour of the plasma or neutron sources different from those originating from fusion. The neutron yield can be correctly correlated through Maxwellian reactivity to ion temperature. The evaluation of error on this measurement is problematic and depends principally on the calibration error and secondly on the error on the fusion cross-section. However, due to the favourable dependence of Maxwellian fusion reactivity on ion temperature, an error of the order of 100% on the neutron yield measurement results in an error of less than 20% on temperature. When neutron sources other than

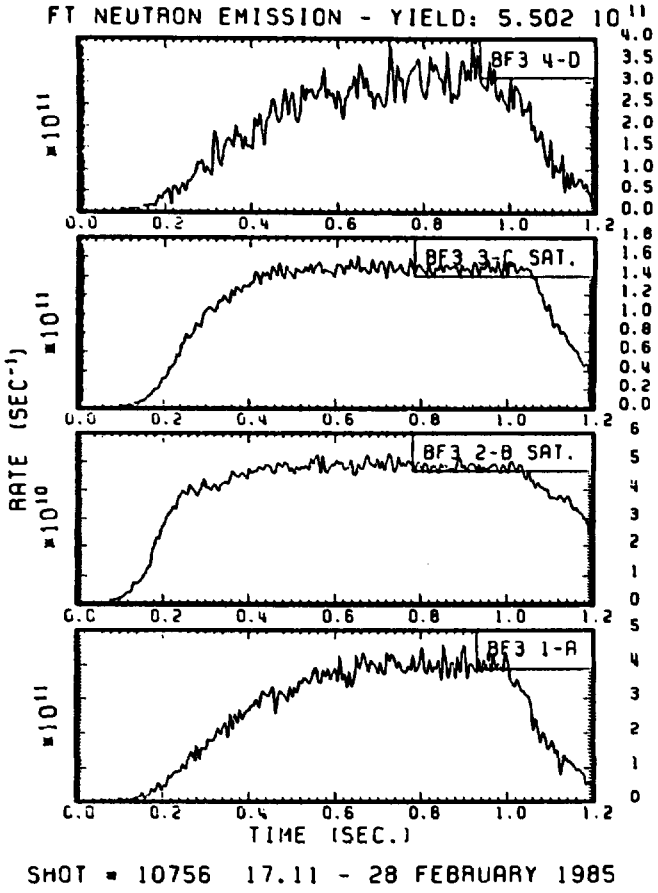


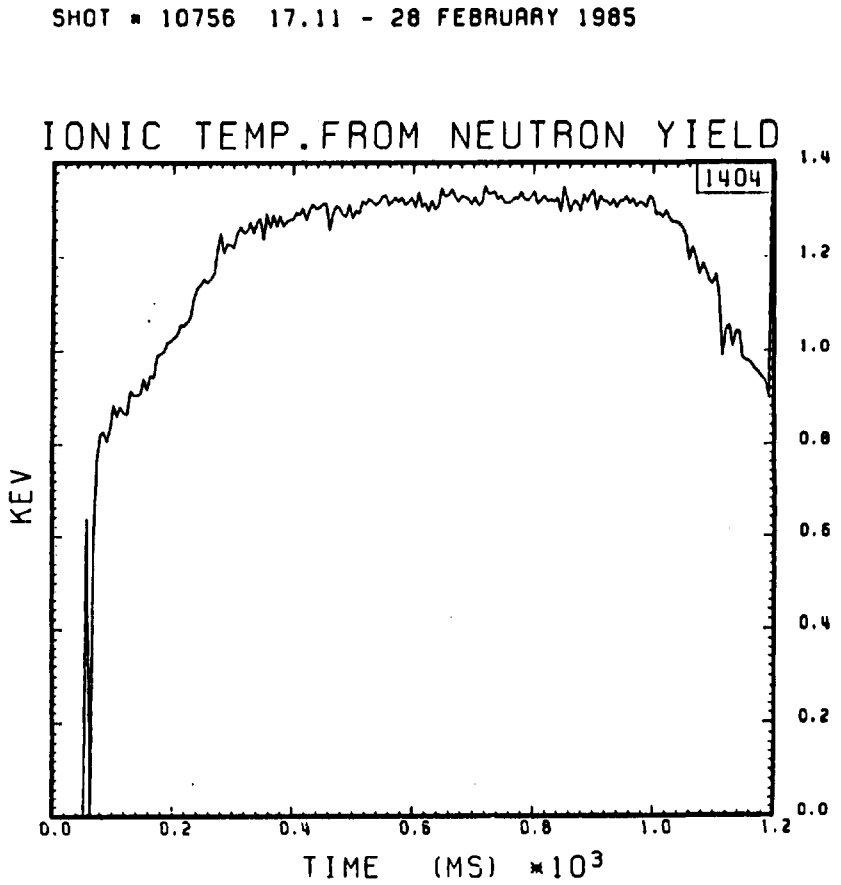


Fig.2 Typical F.T. ohmic discharge.

those from fusion are present this measurement is no longer valid. In particular, we can have neutron production from photonuclear reaction on the materials in the vacuum vessel. As these sources are localized it is possible to discriminate this kind of discharge by anisotropy on neutron emission. In Figure 3 we show the neutron rate measurement from two detectors, one near and the other far from the source of photo-neutrons.

When additional heating is present, deformation of the ion velocity distribution can be induced. On F.T., waves at the lower hybrid frequency (2.45 GHz) are launched in the plasma up to 400 kw of power. We must distinguish different plasma regimes. In Figure 4 we show the neutron rate and ion temperature measurements in the so-called "electron heating regime" ($n_e < 5.10^{13} cm^{-3}$). Here the waves give energy preferentially to electrons and then to ions. The delay between R.F. switch-on and the maximum of ion temperature is compatible with the electron-ion energy exchange time.

Figure 5 shows the behaviour of the neutron rate and ion temperature in the "intermediate regime" ($n_e < 1.2\ 10^{14} cm^{-3}$). Enhancement of the neutron rate is present corresponding to an increase of ion temperature, but an increase of the electron temperature is not observed. We therefore suppose that, in this case, the waves give energy directly to a minority of the ion population creating tails which are not strongly coupled with the bulk plasma. The neutron rate enhancement is due more to a favourable fusion cross-section at high deuteron energy than to a real ion temperature increase. This hypothesis

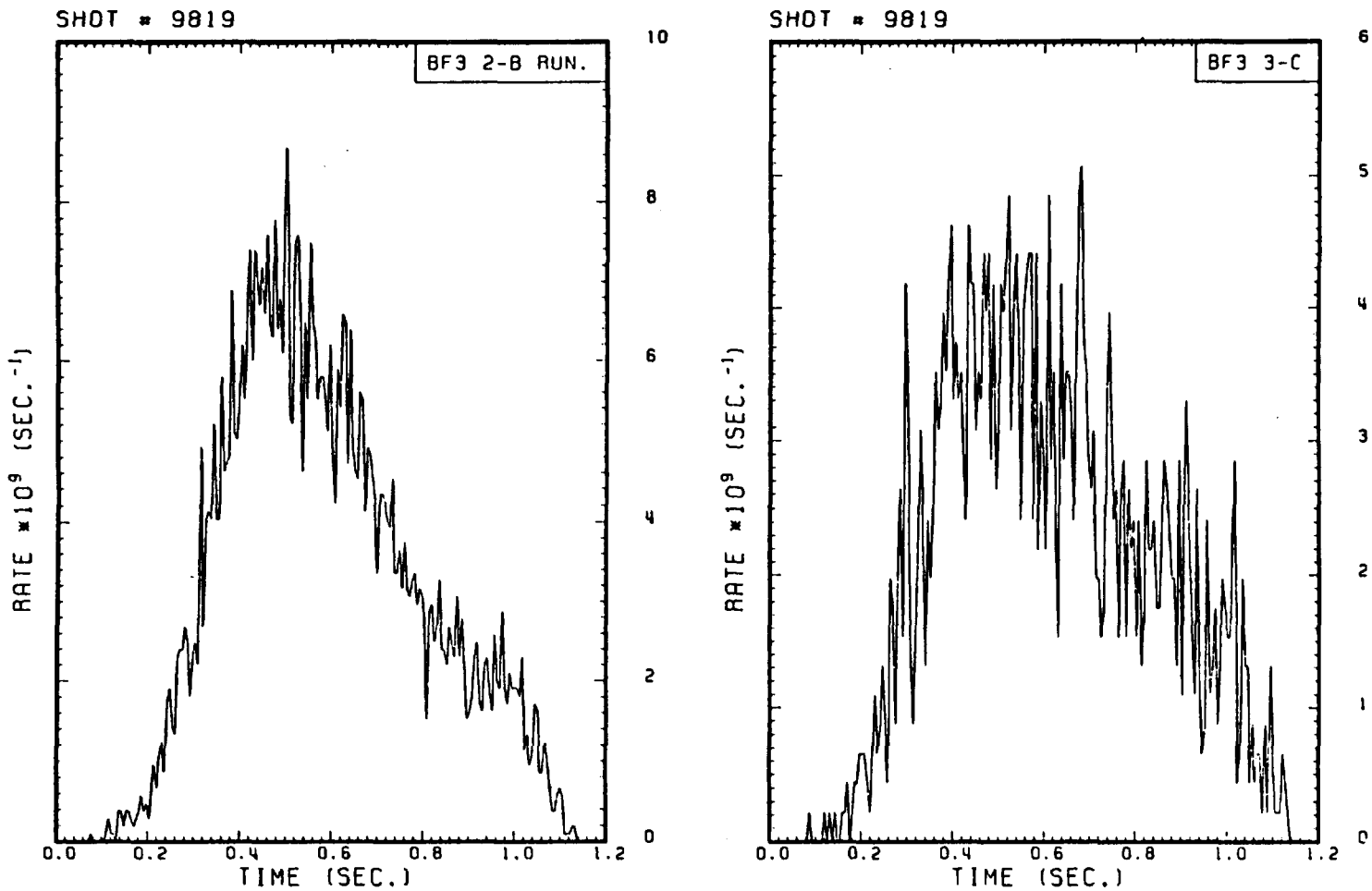


Fig.3 Detector 2-B near photo-neutron source (on left), Detector 3-C far from photo-neutron source (on right).

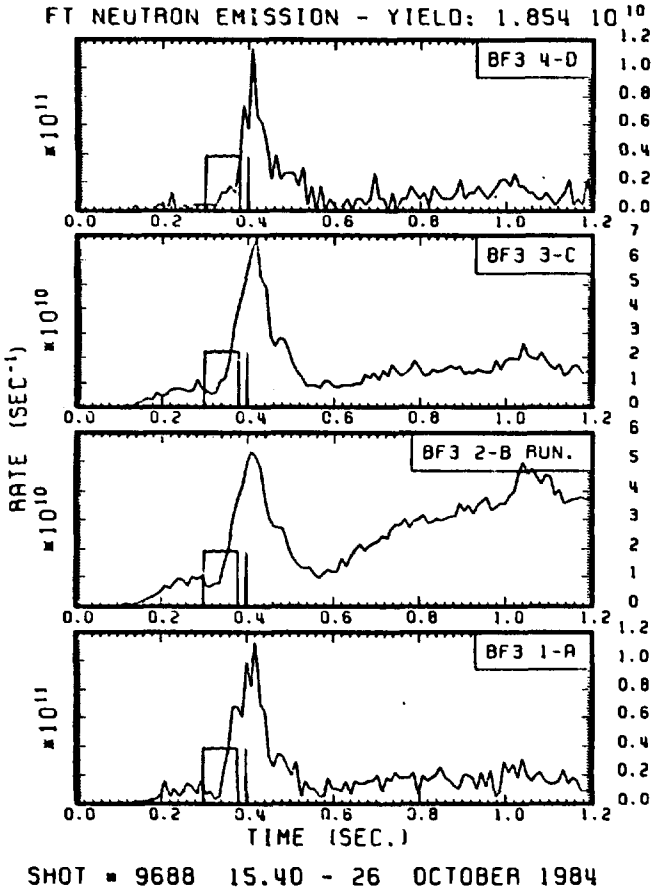


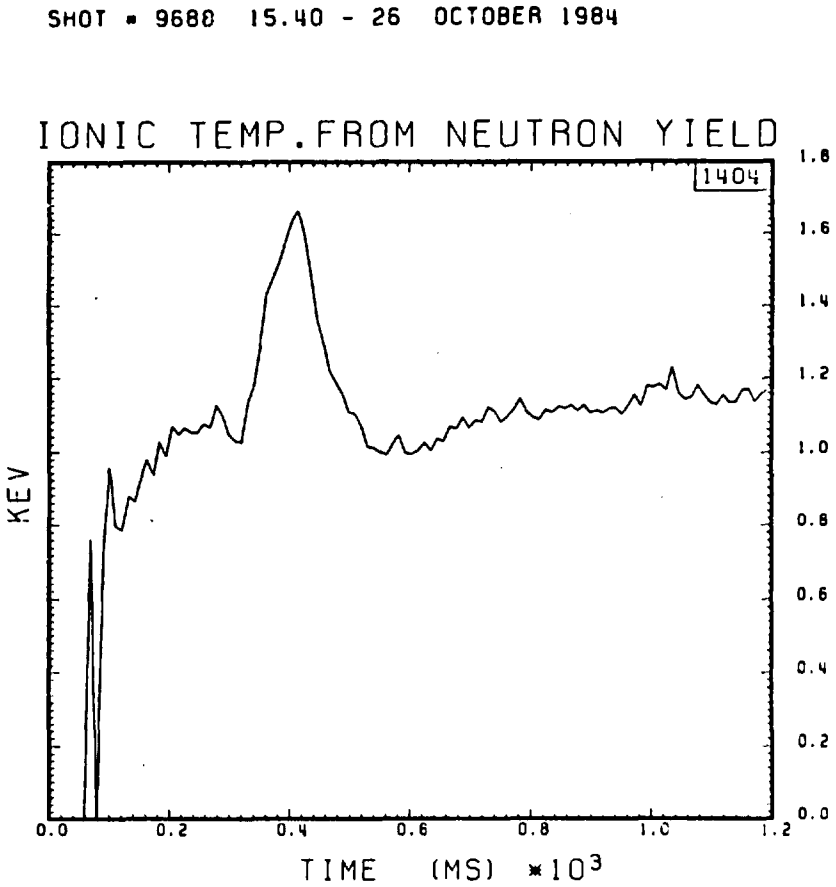


Fig.4 F.T. ohmic discharge plus R.F. additional heating in the "electron heating" regime.

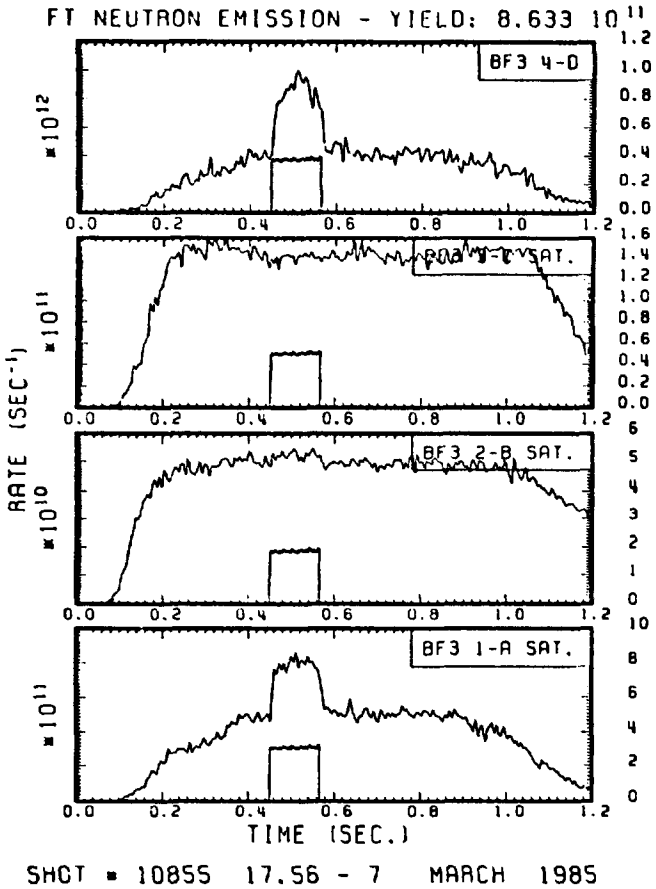


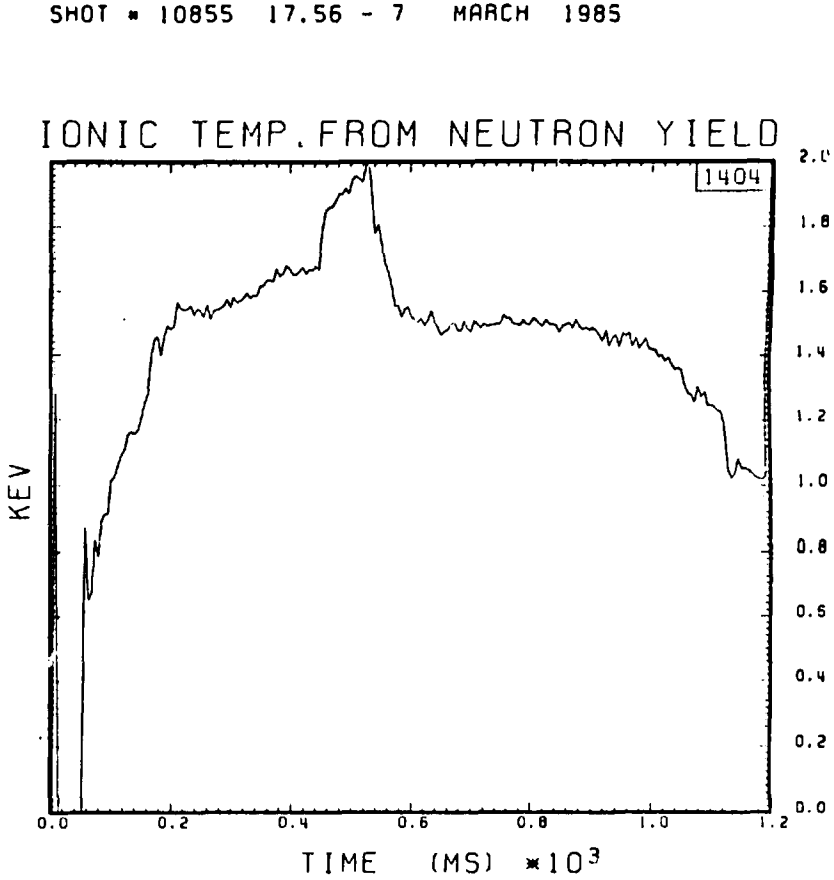


Fig.5 F.T. ohmic discharge plus R.F. additional heating in the "intermediate" regime.

is supported by neutral particles analysis which shows an increase of the neutral flux at higher energy during R.F. injection, but no ion temperature increase, and is coherent with the fast rise and fall time of neutron and neutral fluxes at R.F. switch-on and -off.

In conclusion, Figure 6 shows a particular result of neutron yield measurement which calls attention to a peculiar phenomenon in the plasma. During the R.F. heating programme F.T. worked also in hydrogen and in this case it has neutrons only from photo-production. At R.F. switch-on we observe the disappearance of photo-neutron production. This has been explained [3] by an "anomalous doppler resonance" of relativistic electrons with the lower hybrid waves, which diffuse electrons in phase space, stopping the process of electron acceleration necessary to reach energies sufficient for photo-neutron production. The fall time of neutron production is compatible with the characteristic time of "scattering" of electrons by waves while the growth time of neutron production after R.F. switch-off is compatible with the time necessary for electron acceleration. This phenomenon has also been observed in deuterium discharges at a low level of R.F. power, but it is often hidden by the competing thermonuclear neutron production.

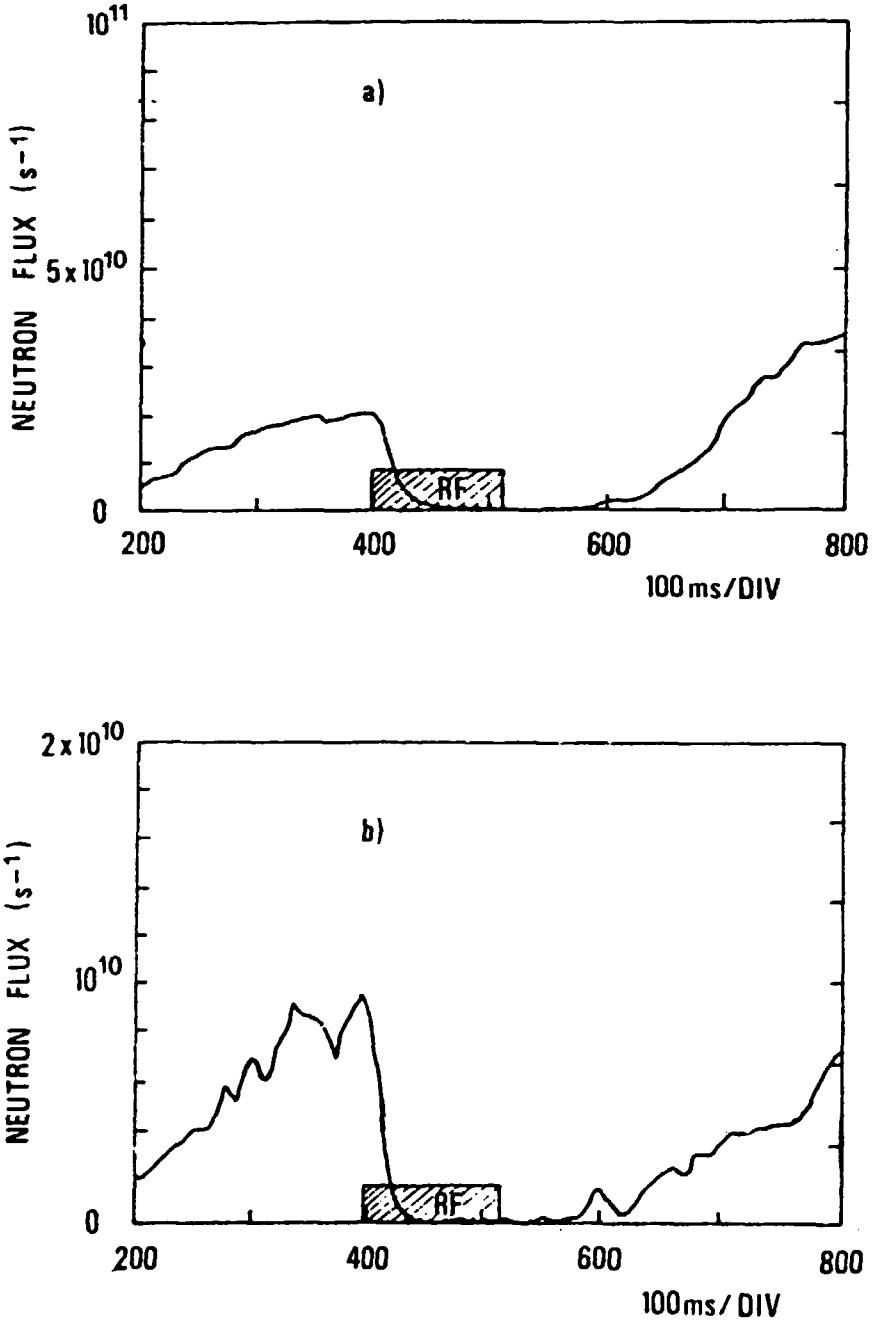


Fig.6 Temporal behaviour of photonuclear neutron emission in hydrogen discharge (a) $\bar{n}_e \approx 3\ 10^{13}\ cm^{-3}$, (b) $\bar{n}_e \approx 6\ 10^{13}\ cm^{-3}$.

References

[1] Grosshoeg G., Nucl. Instr. and Meth., 162 (1979) 125.

[2] Vannucci A., E.N.E.A. Thesis.

[3] Santini F., et al., Phys. Rev. Letters 52 (1984) 1300.

# PRELIMINARY MEASUREMENTS OF THE 14 MeV NEUTRON EMISSION FROM FRASCATI TOKAMAK PLASMA BY ACTIVATION TECHNIQUES

M. Pillon, A. Vannucci*

Associazione EURATOM-ENEA sulla Fusione, C.R.E. Frascati, C.P. 65, 00044 Frascati, Rome, (Italy)

## ABSTRACT

The 1.01 MeV triton burn-up has been investigated in the FT plasma by means of the activation technique. The 14 MeV neutrons produced by triton burn-up have been measured with the activation reaction $Cu^{63}(n,2n)Cu^{62}$ which has a threshold of 10.9 MeV.

## INTRODUCTION

The properties of MeV ions in fusion devices are of interest since ignition requires that charged fusion reaction products be confined long enough for most of their energy to be transferred to the plasma. In an ohmically heated deuterium plasma, 1.01 MeV tritons are produced by the reaction D(d,p)T with a nearly equal probability of 2.45 MeV neutrons from the reaction $D(d,n)He^{3}$. According to the classic theory, the fast tritons born on a contained trajectory, are slowed down to the plasma thermal energy mainly by the electron drag. During slowing-down a frac-

---

* ENEA Student

tion of the tritons produced undergoes the reaction T(d,n)α producing 14 MeV neutrons. Thus, the (D,T)/(D,D) neutron emission ratio can be related to the confinement factor fc of the fast tritons during decelerations by

$$N_{14MeV}/N_{2.5MeV} = fc < P_{DT} > \quad (1)$$

where $<P_{DT}>$ is the average probability of fusion for the confined triton in the deuterium plasma. 1.01 MeV triton burn-up in PLT and PDX tokamaks during several multimegawatts of deuterium neutral beam injection heating has been reported [1,2].

In this paper we describe the measurements of the tritium burn-up in an ohmically heated plasma for single FT discharges and its dependence on the plasma current in the range 450-570 KA. In order to measure the (D,T)/(D,D) neutron emission ratio, it would be desirable to have detectors which are sensitive to 14 MeV and 2.5 MeV neutrons respectively, but insensitive to other radiations. The threshold activation foils provide excellent discrimination from lower-energy neutrons and hard X-rays.

## DETECTION METHODS

The (D,D) neutron emission was measured by four $BF_3$ chambers which has been previously calibrated using indium activation samples while the (D,T) neutrons were measured with copper samples [3]. The measurement of the 14 MeV neutrons is delicate because of the low flux ($\sim 10^3$ $cm^{-2}$ $sec^{-1}$) of these neutrons in the high background of the 2.5 MeV neutrons and possible hard x-rays. The

reaction $^{63}Cu$ (n,2n) $^{62}Cu$, which has a threshold of 10.9 MeV, has a fairly high cross section of 0.44 barn at 14 MeV, which permits, using samples of several hundreds grams, measurements on a single FT discharge.

The $^{62}Cu$ decays into $^{62}Ni$ with a half-life or 9.73 min. by emitting a $\beta^+$. The subsequent 511 keV gamma rays have been measured by a high purity germanium spectrometer. Account has been taken of the activation by epithermal neutrons of $^{64}Cu$ emitting also a $\beta^+$ with a half-life of 12.71 hours.

No hard X-rays are measured at high density discharges ($\bar{n}_e \gtrsim 10^{14}$ cm$^{-3}$) used for activation measurements. However, in order to confirm that the $^{63}Cu(\gamma,n)^{62}Cu$ does not contribute to the 14 MeV neutron counting, we have exposed for a few tens of shots aluminium samples to identical FT discharges, as the $^{24}Na$ produced by the $^{27}Al(n,\alpha)^{24}Na$ reaction cannot be obtained by photonuclear reaction. The impurity content of our samples has been checked by thermal neutron activation and has been found better than $10^{-5}$ for interfering elements.

The self absorption coefficient of the $\gamma$ rays in the sample has been measured [3] for our particular sample--germanium geometry.

The alteration of the 14 MeV neutron flux over the finite dimension of the sample, inserted into the massive structure of the FT toroidal coils and cryostat, has been calculated by means of the ANISN code in cylindrical geometry. Calculations, still under way, by means of a tridimensional numerical code will permit the study of toroidal geometry and non axisymmetric features like the win-

dows and the samples themselves. As a first approximation we have found that the dominant effect is the attenuation of the 14 MeV neutron flux across the material, while the scattered neutrons due to the high threshold of the $^{63}Cu(n,2n)^{62}Cu$ have little effect.

Up to now we have analysed by means of activation about 10 shots with copper and 20 shots with aluminium. The magnetic field was $B_\phi$ = 80 kg and no additional heating was used. In table I the measured ratio (D,T)/(D,D) with the counting statistical error and the other plasma parameters is reported.

In figure 1 this ratio is plotted versus the plasma current. The average fusion probability $\langle P_{DT} \rangle$ (eq. 1) scales in the classic burn-up theory as $\bar{T}_e^{32}$ [4] and the electron temperature in FT has been found to scale with the plasma current as $T_e \propto I_p^{12 \div 32}$ [5]. Using the calculated values of fc from Ref. 6 for the FT aspect ratio A = 4, we can calculate the scaling law of (D,T)/(D,D) with the plasma current. The theory of Ref. 6 predicts a dependence on $fc \propto I_p^{2.4}$ in the range of 450 ÷ 600 KA,

TABLE I

| $\frac{(D,T)}{(D,D)} \times 10^{-3}$ | $I_p$ (KA) | $\bar{n}_e \times 10^{14}$ ($cm^{-3}$) | $\bar{T}_i$ (KeV) | (D,D) x $10^{11}$ ($sec^{-1}$) |
|---|---|---|---|---|
| 1.56±0.282 | 450 | 1.5 | 1.0 | 3.12 |
| 2.43±0.334 | 505 | 2.0 | 1.2 | 10.0 |
| 2.91±0.485 | 520 | 2.2 | 1.1 | 4.83 |
| 2.90±0.419 | 570 | 2.0 | 1.3 | 8.22 |

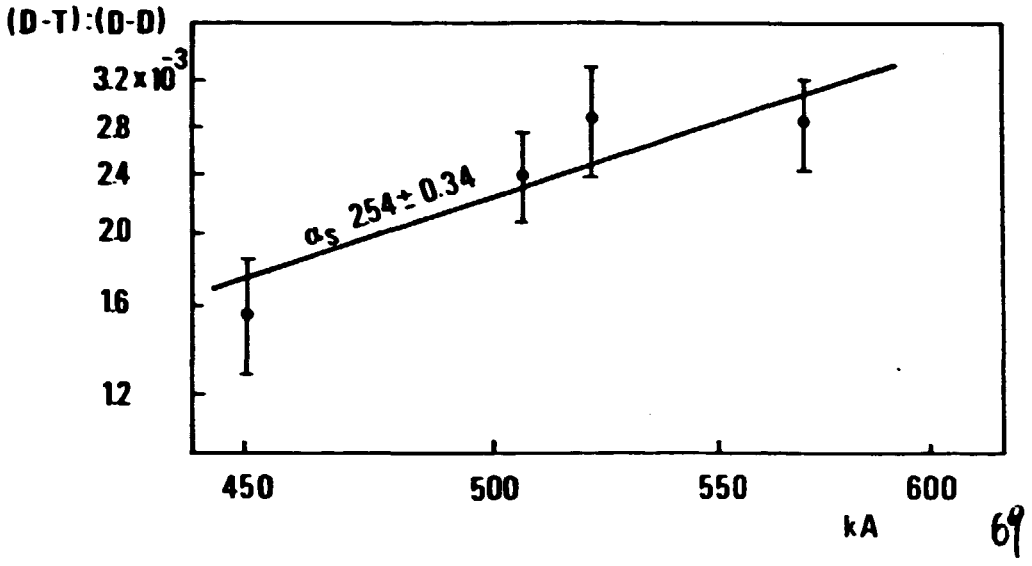


Fig. 1 - (D,T)/(D,D) neutron emission ratio vs plasma current.

so (D,T)/D,D) $\propto I_p^{\alpha t}$ where $\alpha t = 3.15 \div 2.4$. This value is consistent with the experimental one $\alpha_s = 2.54 \pm 0.34$ (Fig. 1).

The sources of uncertainties in the measurements of the (D,T)/(D,D) neutron emission ratio and their uncertainty contributions are reported in Table II.

TABLE II

| Sources of Uncertainties | Uncertainty Contributions |
|---|---|
| Cross section $^{63}Cu(n,2n)^{62}Cu$ | ± 7% |
| Detectory efficiency | ± 5% |
| Gamma self-shielding factor | ± 10% |
| Corrective factor D | ± 50% |
| $BF_3$ calibration | ± 25% |
| Counting statistics | ± 14÷18% |
| Total | ± 60% |

## CONCLUSIONS

In our preliminary results the total experimental error is large and further work should be carried out to reduce it. However we can conclude that our results are consistent with the early measurements on PLT and PDX tokamaks [1,2] and with the classic slowing-down theory. The $^{63}Cu(n,2n)^{62}Cu$ activation reaction has been shown to be a reliable method to study the tritium confinement properties in the FT plasma in a single shot at plasma current level > 450 KA.

## REFERENCES

[1] COLESTOCK, P.L. et al., Phys. Rev. Lett. 43 (1979) 768

[2] HEIDRINK, W.W. et al., Nucl. Fusion 23 (1983) 917

[3] FUBINI, A, et al. ENEA Report, Associazione EURATOM--ENEA sulla Fusione, C.R.E. Frascati, (1985) to be published

[4] SPITZEL, L., Physics of Fully Ionized Gases, Interscienze, New York (1962)

[5] PIERONI, L., et al. Nucl. Fusion 20 (1980) 897

[6] BITTONI, E., et al. Nucl. Fusion 22 (1982) 1675

Edito dall'ENEA, Direzione Centrale Relazioni.
Viale Regina Margherita 125, Roma.
Fotoriproduzione e Stampa Arti Grafiche S. Marcello - Roma